Marine Geology xxx (2012) xxx–xxx

Contents lists available at SciVerse ScienceDirect

Marine Geology

journal homepage: www.elsevier.com/locate/margeo

Widespread and progressive seafloor-sediment failure following volcanic debris avalanche emplacement: Landslide dynamics and timing offshore Montserrat, Lesser Antilles

S.F.L. Watt [a,*], P.J. Talling [b], M.E. Vardy [a], D.G. Masson [b], T.J. Henstock [a], V. Hühnerbach [b], T.A. Minshull [a], M. Urlaub [a], E. Lebas [c], A. Le Friant [c], C. Berndt [b,d], G.J. Crutchley [d], J. Karstens [d]

[a] National Oceanography Centre Southampton, University of Southampton, European Way, Southampton SO14 3ZH, UK
[b] National Oceanography Centre, European Way, Southampton SO14 3ZH, UK
[c] Institut de Physique du Globe de Paris, UMR 7154, CNRS, Paris, France
[d] Helmholtz Centre for Ocean Research Kiel, GEOMAR, 24148 Kiel, Germany

ARTICLE INFO

Article history:
Received 9 January 2012
Received in revised form 8 August 2012
Accepted 9 August 2012
Available online xxxx

Communicated by D.J.W. Piper

Keywords:
seafloor-sediment slide
progressive landslide
frontal confinement
undrained loading
volcanic debris avalanche
Montserrat

ABSTRACT

Landslides associated with flank collapse are volumetrically the most significant sediment transport process around volcanic islands. Around Montserrat, in the Lesser Antilles, individual landslide deposits have volumes (1 to 20 km^3) that are up to two orders of magnitude larger than recent volcanic dome collapses (up to 0.2 km^3). The largest landslide deposits were emplaced in at least two stages, initiated by the emplacement of volcanic debris avalanches which then triggered larger-scale failure of seafloor sediment, with deformation propagating progressively downslope for up to 30 km on gradients of <1°. An unusually detailed seismic, side-scan sonar and bathymetric dataset shows that the largest landslide off Montserrat (forming Deposit 8) incorporated ~70 m of in-situ sediment stratigraphy, and comprises ~80% seafloor sediment by volume. Well-preserved internal bedding and a lack of shortening at the frontally-confined toe of the landslide, shows that sediment failure involved only limited downslope transport. We discuss a range of models for progressively-driven failure of in-situ bedded seafloor sediment. For Deposit 8 and for comparable deposits elsewhere in the Lesser Antilles, we suggest that failure was driven by an over-running surface load that generated excess pore pressures in a weak and deforming undrained package of underlying stratigraphy. A propagating basal shear rupture may have also enhanced the downslope extent of sediment failure. Extensive seafloor-sediment failure may commonly follow debris avalanche emplacement around volcanic islands if the avalanche is emplaced onto a fine-grained parallel-bedded substrate. The timing of landslides off Montserrat is clustered, and associated with the deposition of thick submarine pyroclastic fans. These episodes of enhanced marine volcaniclastic input are separated by relatively quiescent periods of several 100 ka, and correspond to periods of volcanic edifice maturity when destructive processes dominate over constructive processes.

© 2012 Elsevier B.V. All rights reserved.

1. Introduction

Deep-seated flank collapses on volcanic islands produce some of the largest mass transport events on Earth's surface. Individual submarine landslide deposit volumes in the Canary Islands and Hawaii exceed 500 km^3 (Moore et al., 1994; Masson et al., 2002), while landslide deposits off Dominica, in the Lesser Antilles arc (Deplus et al., 2001; Le Friant et al., 2002), cover an area of 3500 km^2. The scale of these events far exceeds the largest known subaerial volcanic landslide deposit, which occurred at Mount Shasta and had a volume of >45 km^3 and an area of 675 km^2 (Crandell, 1989), and is two orders of magnitude larger than the collapse of Mount St. Helens in 1980, which deposited 2.8 km^3 of material over 60 km^2 (Voight et al., 1983).

The largest landslides from volcanic islands may generate damaging tsunamis on an ocean-basin scale (Løvholt et al., 2008; Waythomas et al., 2009). The magnitude of such tsunamis is a source of debate (Ward and Day, 2001; Masson et al., 2006); accurate magnitude assessment requires a better understanding of landslide emplacement processes (cf. Watt et al., 2012). We are yet to monitor a major volcanic-island collapse in progress, and our understanding therefore relies on the study of past landslide deposits.

Here we investigate landslide emplacement around Montserrat, in the Lesser Antilles volcanic arc, where ten landslide deposits have been identified previously in the SE offshore sector (Le Friant et al., 2004; Lebas et al., 2011). We focus on the largest of these landslides,

* Corresponding author. Tel.: +44 2380 596614; fax: +44 2380 593052.
E-mail address: sebastian.watt@noc.soton.ac.uk (S.F.L. Watt).

0025-3227/$ – see front matter © 2012 Elsevier B.V. All rights reserved.
http://dx.doi.org/10.1016/j.margeo.2012.08.002

Please cite this article as: Watt, S.F.L., et al., Widespread and progressive seafloor-sediment failure following volcanic debris avalanche emplacement: Landslide dynamics and timing offshore Montserrat,..., Marine Geology (2012), http://dx.doi.org/10.1016/j.margeo.2012.08.002

named Deposits 2 and 8. At ~9 and ~20 km^3 respectively, they represent by far the largest-volume events at Montserrat in the last million years. We provide a detailed examination of landslide deposit constituents and structures, and use this to give new insights into submarine landslide emplacement, extent and timing.

This work builds on previous geophysical investigations that have focussed on determining the local landslide deposit stratigraphy (Deplus et al., 2001; Le Friant et al., 2004; Kenedi et al., 2010; Lebas et al., 2011). The reader is referred to Lebas et al. (2011) for an overview of the landslide deposit stratigraphy and parameters SE of Montserrat. The current contribution also extends the results of Watt et al. (2012), who discussed the implications of combined volcanic-flank and seafloor-sediment failure (based on structures in Deposit 2) for tsunami generation. Direct sampling of marine sediments around Montserrat was limited to short (<5 m) cores (Reid et al., 1996; Le Friant et al., 2008; Trofimovs et al., 2010), until drilling

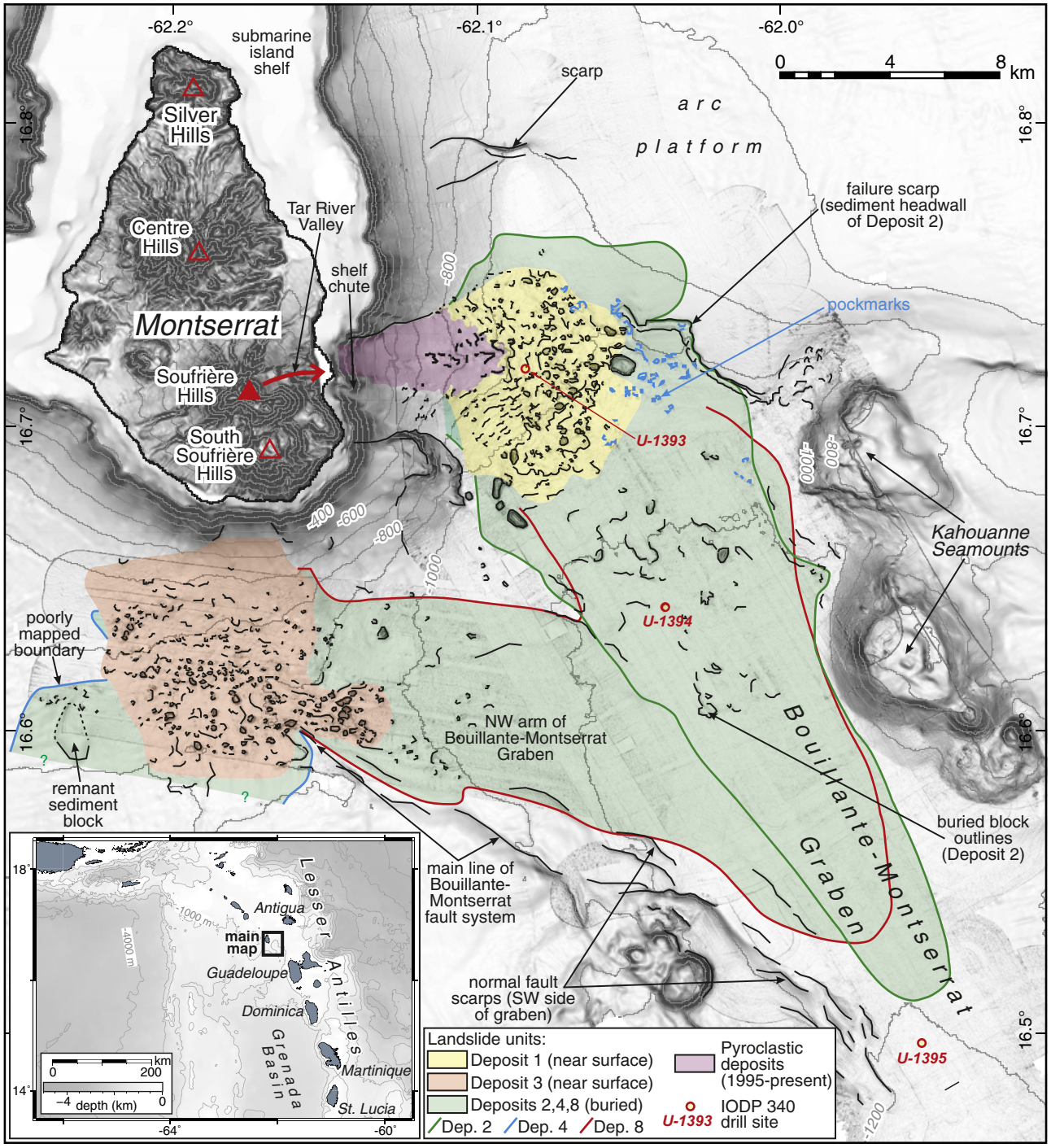

Fig. 1. Montserrat and the surrounding seafloor, showing marine landslide deposit outlines. Outlines of landslide deposits are inferred from JC45/46 data, and the extent of recent pyroclastic deposits (1995–present eruption of Soufrière Hills) is from Le Friant et al. (2010). Seafloor morphological features are outlined, highlighting the blocky surfaces of landslide Deposits 1 and 3. The inset map shows the regional location of Montserrat, in the Lesser Antilles volcanic arc.

Please cite this article as: Watt, S.F.L., et al., Widespread and progressive seafloor-sediment failure following volcanic debris avalanche emplacement: Landslide dynamics and timing offshore Montserrat,..., Marine Geology (2012), http://dx.doi.org/10.1016/j.margeo.2012.08.002

ARTICLE IN PRESS

at four core sites during IODP 340, in early 2012 (Fig. 1). Much remains to be learnt from the offshore record about the history of volcanism and landslide processes.

1.1. Aims and outline

Based on a structural interpretation, we show that the largest landslide deposits around Montserrat mainly comprise seafloor sediment, rather than material from the volcanic edifice (Sections 4 and 5). In light of this, we discuss emplacement processes in Section 6, aiming to elucidate the mechanisms of seafloor-sediment failure and propagation, factors controlling the style of failure, and whether similar processes have occurred elsewhere. We then discuss generalised models of seafloor-sediment failure around volcanic islands. Finally, in Section 7 we use sediment accumulation rates to estimate landslide ages and assess how landslide timing relates to the long-term evolution of Montserrat.

1.2. Terminology

We refer to marine sediment deposited directly from a volcanic source (such as pyroclastic density currents or volcanic flank collapse) as volcaniclastic (Manville et al., 2009), and to all remaining material as seafloor sediment, emphasising its transportation through non-volcanic processes, even if sediment clasts are volcanic in origin. Thus, a single landslide deposit may include both volcaniclastic blocks from an edifice collapse, and seafloor sediment incorporated into the final deposit.

Landslide is used here as a generic term, describing any gravity-driven failure of rock or sediment, without implications for the processes characterising movement. The term debris avalanche (cf. Siebert, 1984) is used solely to describe blocky landslides originating directly from collapse of the subaerial and/or submarine island flanks (note that this potentially includes non-volcanic rock, such as carbonate shelf material).

2. Geological setting and background

Relationships between active volcanism, tectonics and marine sedimentation have been widely investigated in the Lesser Antilles island arc (Sigurdsson et al., 1980; Carey and Sigurdsson, 1984; Reid et al., 1996; Boudon et al., 2007; Feuillet et al., 2010). In particular, since Soufrière Hills volcano began erupting on Montserrat in 1995, numerous studies have created a benchmark dataset for this andesitic volcano (e.g., Druitt and Kokelaar, 2002).

The oldest subaerial rocks dated from Montserrat (2.6 Ma) are from the heavily eroded Silver Hills volcano, at the northern end of the island (Harford et al., 2002) (Fig. 1). Younger volcanism migrated progressively southwards, first to the Centre Hills volcano (<0.95–0.55 Ma), and then to the South Soufrière Hills–Soufrière Hills complex (<0.17 Ma) (Harford et al., 2002). The above dates do not cover submarine stages of volcanism, and may also be incomplete due to erosion or burial of older subaerial rocks.

The 1995–present eruption of Soufrière Hills has been characterised by cyclic growth and partial collapse of an andesitic lava dome (Druitt and Kokelaar, 2002; Wadge et al., 2010). Approximately 65% of the erupted material has entered the sea (Le Friant et al., 2010), mostly via collapse-generated pyroclastic density currents. Their deposits are likely to be heterogeneous and coarse (recent subaerial pyroclastic deposits contain metre-scale blocks; Cole et al., 2002), and have formed a submarine lobe (~0.8 km^3) east of Soufrière Hills (Fig. 1), with associated turbidites that extend at least 40 km offshore (Trofimovs et al., 2006, 2008, 2011; Le Friant et al., 2009, 2010). Similar processes are likely to have been a significant source of marine sediment during any period of active volcanism on Montserrat.

2.1. Morphology of the study area

A submarine shelf is cut into the flanks of Montserrat at ~90 m depth (Fig. 1) (Le Friant et al., 2004). A prominent shelf chute, off the Tar River Valley (Fig. 1), provided a route for recent pyroclastic deposits (Fig. 3) as well as older landslides (Le Friant et al., 2004; Lebas et al., 2011). Further north, gullies at the shelf edge (Fig. 2) have carried sediment flows offshore, including deposits from a dome collapse in February 2010.

East of Centre Hills and Silver Hills, Montserrat is constructed on an arc platform at ~800 m depth. South of here, the seafloor deepens into the asymmetrical Bouillante-Montserrat Graben, bounded on the NE side by small normal-fault offsets and the Kahouanne Seamounts (Feuillet et al., 2010) (Fig. 1). The graben seafloor, at ~1100 m (and shallower south of Montserrat), gradually deepens to the south-east. Prominent NW–SE scarps of the Bouillante-Montserrat fault system (Feuillet et al., 2010) mark the SW side of the graben, while further to the south-west, the seafloor deepens gradually into the back-arc Grenada Basin (Reid et al., 1996) (Fig. 1).

The arc platform is draped by well-bedded sediments, forming a monocline dipping into the northern edge of the Bouillante-Montserrat Graben. The smooth seafloor here suggests a recent dominance of turbidites and hemipelagic sedimentation (Trofimovs et al., 2010). Two scarps are prominent on the arc platform (Figs. 1, 2 and 4). The origin of the northern scarp (70 m deep and 2.6 km long) is uncertain, but it may mark the eastern edge of a fault continuing to the south of Silver Hills. A second scarp marks the NE edge of the graben, and is the headwall of a sediment failure that fed part of Deposit 2 (Watt et al., 2012).

2.2. Offshore landslide deposit stratigraphy

Of the landslide deposits described by Lebas et al. (2011), Deposits 1, 2, 3, 4 and 8 are discussed here. We focus primarily on the largest, Deposits 2 and 8, which are structurally complex. We also consider how Deposit 4 is related to Deposit 8. All of the landslide deposits appear to have been associated with volcanic collapse, since they contain large structureless blocks dispersed from a source around the island flanks (Lebas et al., 2011). None of the deposits have been dated directly; correlation with subaerial units suggests Deposit 1 may be as young as 2 ka (Boudon et al., 2007), while Lebas et al. (2011) used assumed sedimentation rates to suggest Deposit 8 formed at ~900 ka.

Deposits 1 and 3 are relatively young, and form bathymetrically distinct sub-circular blocky fans (Fig. 1). Deposit 1 derives from a collapse east of Soufrière Hills, fed through the shelf chute, and Deposit 3 originates from the southern side of Montserrat (Le Friant et al., 2004; Lebas et al., 2011). The largest blocks are ~200 m across in Deposits 1 and 3, standing 50 m above the surrounding seafloor. A few much larger blocks (up to 900 m across) protrude 100 m above the seafloor at the outer edge of Deposit 1 (Fig. 4). These may form part of an older unit, Deposit 2.

Deposit 2 lies below Deposit 1 and is more elongate, extending over 30 km into the Bouillante-Montserrat Graben (Fig. 1). In the centre of Deposit 2, partially buried hummocks (Fig. 3), defining irregular marginal banks (cf. Watts and Masson, 2001), cover ~100 km^2 and reach ~22 km offshore (Fig. 3). The large scale of these hummocks, relative to the blocks of Deposit 1, may reflect a deeper-seated and larger-volume volcanic collapse. The outer part of Deposit 2 is smooth surfaced, and extends 12 km downslope beyond the hummocky field. Over this part of the deposit, the seafloor gradient is <0.5° (Fig. 3).

Deposit 4 lies below Deposit 3, and was also derived from a collapse on the south side of Montserrat (Le Friant et al., 2004; Lebas et al., 2011). Immediately east of Deposit 4 lies one lobe of Deposit 8, which extends across the western and northern arms of the

Please cite this article as: Watt, S.F.L., et al., Widespread and progressive seafloor-sediment failure following volcanic debris avalanche emplacement: Landslide dynamics and timing offshore Montserrat,..., Marine Geology (2012), http://dx.doi.org/10.1016/j.margeo.2012.08.002

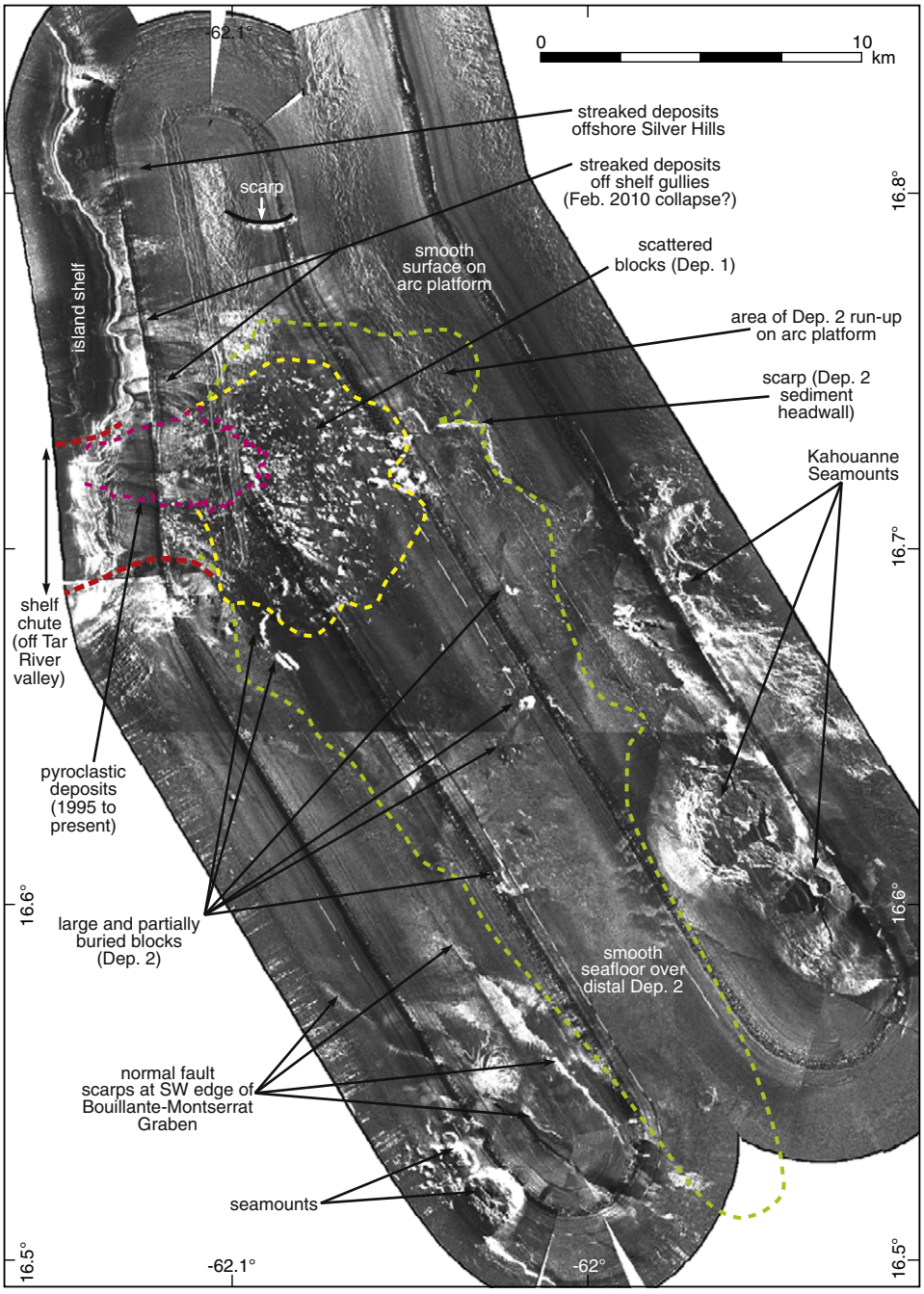

Fig. 2. Interpreted TOBI sidescan sonar (30 kHz) image of the seafloor east of Montserrat, highlighting surficial topographic, structural and sedimentary features.

Bouillante-Montserrat Graben. Based on its burial depth, Lebas et al. (2011) concluded that Deposit 8 originated from a collapse of Centre Hills.

3. Methods

The scale of landslide deposits SE of Montserrat (total area ~300 km^2) and the relatively shallow water depths (~1000 m) permit the collection of a dense coverage of high-resolution geophysical data. Here, we principally use two-dimensional (2D) seismic reflection profiles (vertical resolution <5 m) (Fig. 5), collected on the RRS James Cook JC45/46 research cruise (April to May 2010), to investigate the upper few hundred metres of stratigraphy south and east of Montserrat. In addition, we use JC45/46 sidescan sonar data, swath bathymetry, chirp sub-bottom profiles and a three-dimensional (3D) seismic volume, as well as older 2D seismic profiles (vertical resolution >10 m) from the AGUADOMAR, CARAVAL and SEA-CALIPSO cruises (Deplus et al., 2001; Le Friant et al., 2004; Kenedi et al., 2010) (Fig. 5).

3.1. JC45/46 2D seismic reflection data

The JC45/46 2D seismic profiles have a total track length of 370 km. The seismic source was a generator–injector air gun (2 identical Sercel GI guns; 4916 cm^3 total volume; firing pressure 19 MPa; firing interval 7.0 s), towed 21 m behind the ship at a 3 m depth, with a 60 channel streamer (1 m group spacing; 1 m depth). Ship speed throughout the

Please cite this article as: Watt, S.F.L., et al., Widespread and progressive seafloor-sediment failure following volcanic debris avalanche emplacement: Landslide dynamics and timing offshore Montserrat,..., Marine Geology (2012), http://dx.doi.org/10.1016/j.margeo.2012.08.002

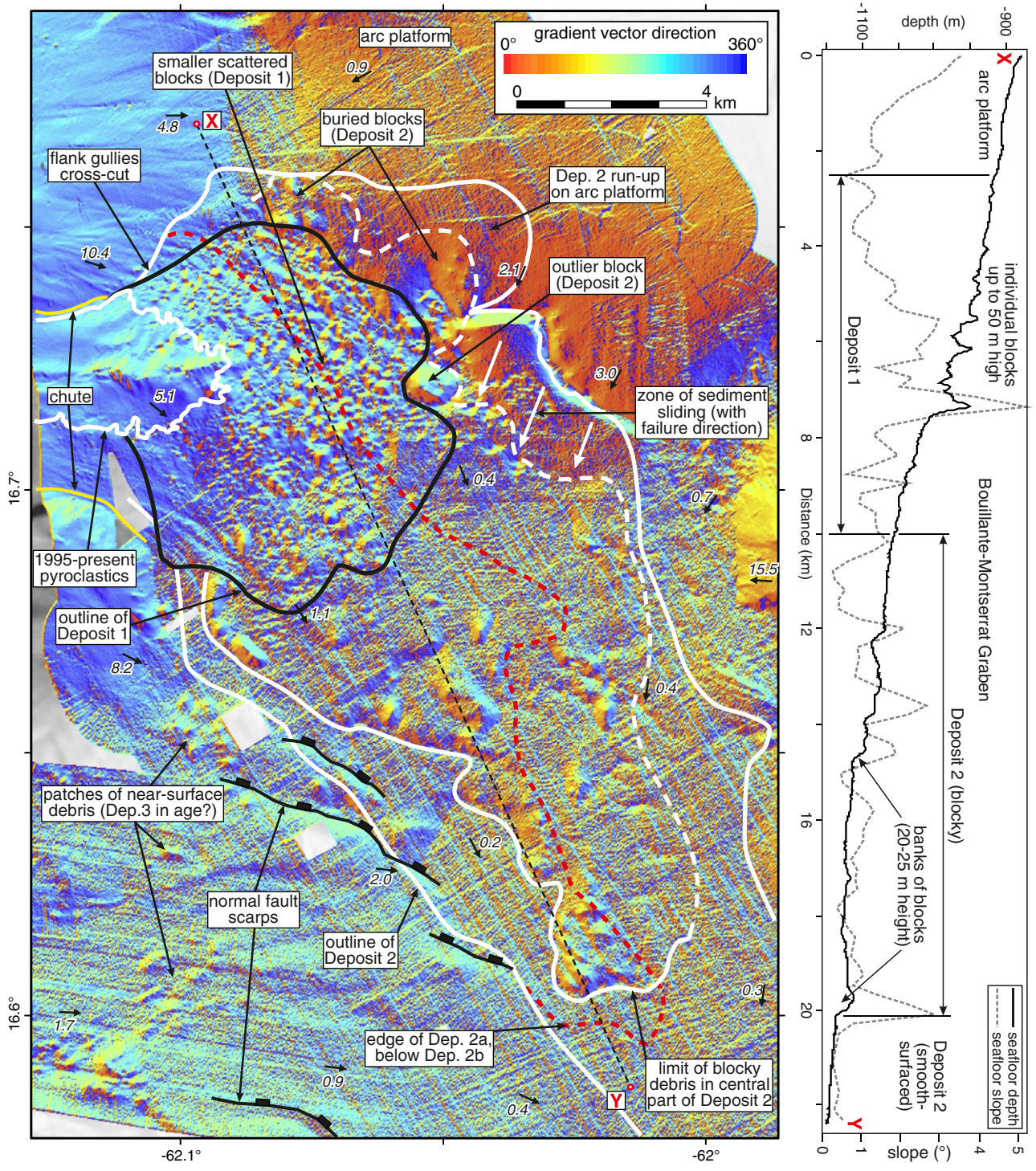

Fig. 3. Main panel: bathymetry east of Montserrat (20 m grid), shaded by the direction of the seafloor vector gradient and highlighting morphological features. The seafloor gradient (in degrees) at selected points is shown by small arrows. Large volcanic blocks, with a coherent slope, are prominent in the central part of the buried Deposit 2. Right: depth and slope profiles down the graben. The slope profile is smoothed (200 m grid) relative to the depth profile (20 m grid).

survey was ~4 knots. Sampling was at 1 ms intervals, recording for 3.0 s. The source bandwidth was 50–150 Hz. Seismic profiles were processed using an adaptive deconvolution, bandpass filtering (10–20–300–350 Hz) and a time-varying gain correction, followed by stacking at 5 m common depth point intervals and a post-stack f–k Stolt migration (linear vertical velocity gradient; 1490 m s^{-1} at seafloor to 2500 m s^{-1} at 1.5 s two-way-time below seafloor).

The short JC45/46 streamer recorded limited reflection move-out, and a precise seismic velocity model cannot be produced. For this reason, 2D seismic profiles and isopach maps are shown in two-way time. However, we use a seismic velocity of 2000 m s^{-1} (based on modelled velocities for the upper 500 m of sediment from travel-time tomography; Paulatto et al., 2010) to provide indicative volumes and thicknesses throughout this paper. An error of ~10% is likely for

Please cite this article as: Watt, S.F.L., et al., Widespread and progressive seafloor-sediment failure following volcanic debris avalanche emplacement: Landslide dynamics and timing offshore Montserrat,..., Marine Geology (2012), http://dx.doi.org/10.1016/j.margeo.2012.08.002

ARTICLE IN PRESS

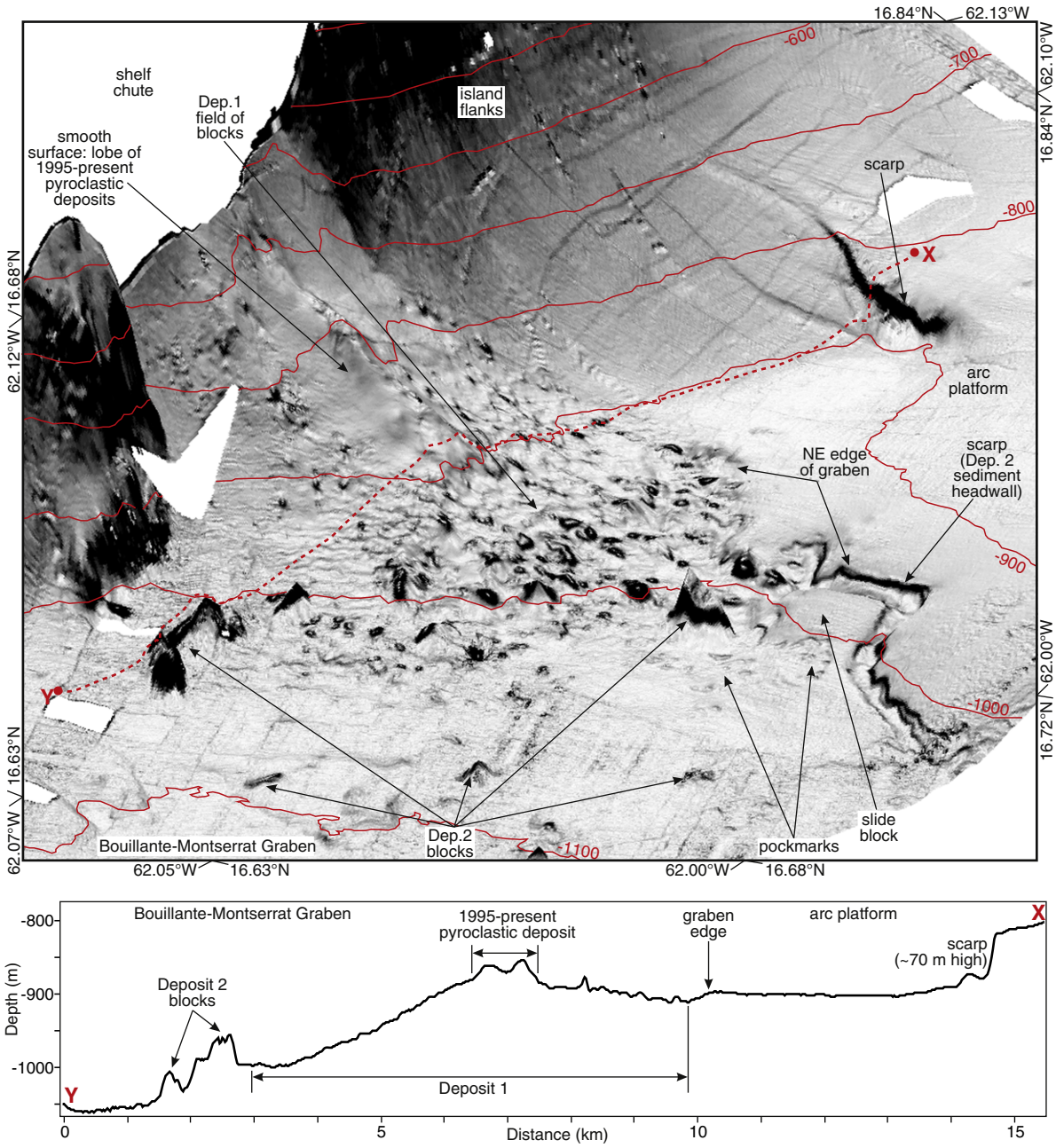

Fig. 4. Main panel: three-dimensional gradient-shaded swath bathymetry (JC45/46) showing Deposit 1 and the head of Deposit 2, viewed from the SE (looking from the northern Kahouanne seamount towards the shelf chute; Fig. 1). Lower panel: N–S surface profile across Deposit 1.

our depth estimates, given both model uncertainties and potential lateral velocity variations.

3.2. Other geophysical data

Multi-beam swath bathymetry (Kongsberg Simrad EM 120; 12 kHz nominal frequency) was collected throughout JC45/46, and processed using velocities from four sound velocity profiles to give a final grid at 20 m spacing. A deep-towed sidescan sonar survey (TOBI; 30 kHz) (Fig. 2) covered the area of the main 2D seismic grid.

Chirp sub-bottom profiler (SBP) data were processed by: stacking the three coincident beams into a single trace; bandpass filtering (2.5–3.0–6.5–7.0 kHz); correlating with the theoretical chirp sweep (linear sweep from 1.5 to 7.0 kHz) to collapse reflections to the Klauder wavelet; and boosting signal-to-noise using a minimum-phase predictive deconvolution and amplitude recovery. On chirp SBP profiles, which image the shallowest sediment (<30 m), we use a velocity of 1500 m s^{-1} to provide a depth scale.

4. Results

4.1. Seismic facies

The stratigraphy SE of Montserrat is shown in profiles down and across the Bouillante-Montserrat Graben in Figs. 6 and 7. This stratigraphy can be interpreted initially by defining three seismic facies (Figs. 8 and 9).

Please cite this article as: Watt, S.F.L., et al., Widespread and progressive seafloor-sediment failure following volcanic debris avalanche emplacement: Landslide dynamics and timing offshore Montserrat,..., Marine Geology (2012), http://dx.doi.org/10.1016/j.margeo.2012.08.002

ARTICLE IN PRESS

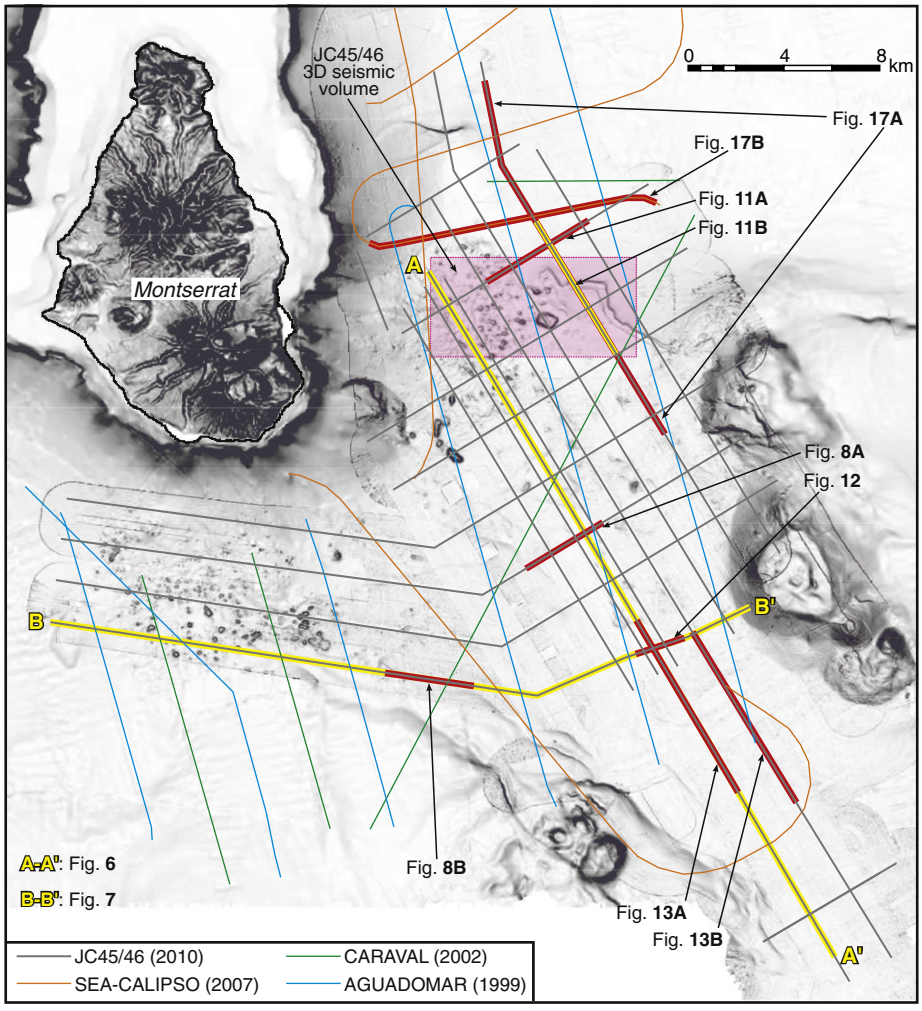

Fig. 5. 2D seismic profile coverage used in this paper, showing four different datasets and their collection dates (Deplus et al., 2001; Le Friant et al., 2004; Kenedi et al., 2010). Line sections used in subsequent figs. are highlighted in red or yellow. The principal dataset used here is that from JC45/46, with older data used for correlation. (For interpretation of the references to colour in this figure legend, the reader is referred to the web version of this article.)

4.1.1. Seafloor-sediment facies

The material filling much of the Bouillante-Montserrat Graben is seismically imaged as laterally continuous beds with generally consistent amplitudes. We term this the seafloor-sediment facies, and interpret it as being fine grained, parallel bedded and relatively homogeneous. The full complexity of the seafloor sediment cannot be resolved in our seismic data: the short (5 m) cores described by Trofimovs et al. (2010) contain multiple interbedded turbidites and hemipelagic intervals, but the thickness of these cores lies only within the first seafloor reflection (Fig. 6).

4.1.2. Pyroclastic facies

The pyroclastic facies is characterised by lenticular or laterally discontinuous high-amplitude bedded reflections (Fig. 8), in packages that taper away from the island flanks (Fig. 9). The 1995–present pyroclastic deposits offshore the Tar River Valley have this character, as does the package separating Deposits 1 and 2 (Fig. 6) and that overlying parts of Deposits 4 and 8 (Fig. 7). By analogy, we suggest these units were deposited during periods of eruptive activity and represent stacked volcaniclastic flow deposits (e.g., from partial dome collapses). Such deposits may accumulate rapidly; the 1995–present eruption has formed 95-m thick offshore deposits in fifteen years (Le Friant et al., 2010). Although the pyroclastic facies is likely to contain interbedded seafloor sediment, this is in insufficient proportions to be seismically imaged.

4.1.3. Landslide facies

The landslide facies may be divided into two types. The first facies contains convex-upwards rounded reflections, diffraction hyperbolae and wavy or broken reflections, often with high amplitudes. This facies occurs nearer the island flanks and is associated with an irregular deposit surface. We interpret it as a deposit containing large blocks sourced from volcanic flank collapses (cf. Le Friant et al., 2004; Lebas et al., 2011). The second facies is chaotic to transparent, in some cases with low amplitude bedded or deformed reflections, and associated with smooth deposit surfaces. We interpret it as finer grained material, and suggest that the bedded reflections represent deformed seafloor sediment. More transparent intervals may indicate greater sediment disaggregation or deposits of fine-grained volcaniclastic material. In places, the landslide facies has an intermediate character, which we interpret as a mix of volcanic blocks with a relatively large proportion of finer sediment.

The landslide facies types are well illustrated in Fig. 8. Firstly, continuous bright reflections break up Deposits 2 and 8 into sub-units (2a, 2b and 8a–c). Both sub-units of Deposit 2 have a similar character: relatively high-amplitude curved or deformed reflections suggest a mix of volcanic blocks and seafloor sediment. The lower two sub-units of

Please cite this article as: Watt, S.F.L., et al., Widespread and progressive seafloor-sediment failure following volcanic debris avalanche emplacement: Landslide dynamics and timing offshore Montserrat,..., Marine Geology (2012), http://dx.doi.org/10.1016/j.margeo.2012.08.002

ARTICLE IN PRESS

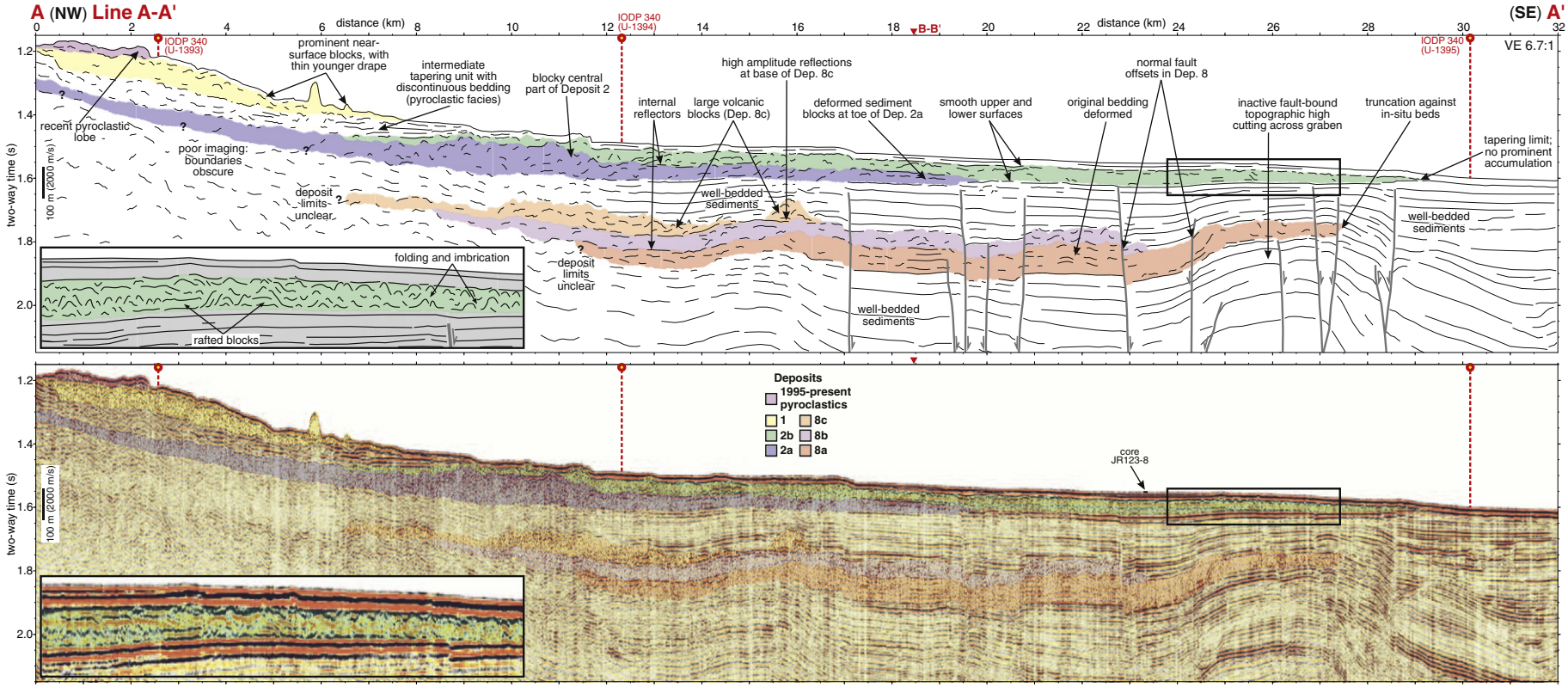

Fig. 6. Interpreted 2D seismic profile (air gun source) down the Bouillante-Montserrat Graben (location in Fig. 5), showing the landslide deposits discussed in the text. IODP 340 drill sites are also shown, as is core JR123-8 (Trofimovs et al., 2010), for comparison. The inset in the lower profile shows detail of interpreted sediment deformation structures within the distal part of Deposit 2b.

Please cite this article as: Watt, S.F.L., et al., Widespread and progressive seafloor-sediment failure following volcanic debris avalanche emplacement: Landslide dynamics and timing offshore Montserrat,..., Marine Geology (2012), http://dx.doi.org/10.1016/j.margeo.2012.08.002

Please cite this article as: Watt, S.F.L., et al., Widespread and progressive seafloor-sediment failure following volcanic debris avalanche emplacement: Landslide dynamics and timing offshore Montserrat,..., Marine Geology (2012), http://dx.doi.org/10.1016/j.margeo.2012.08.002

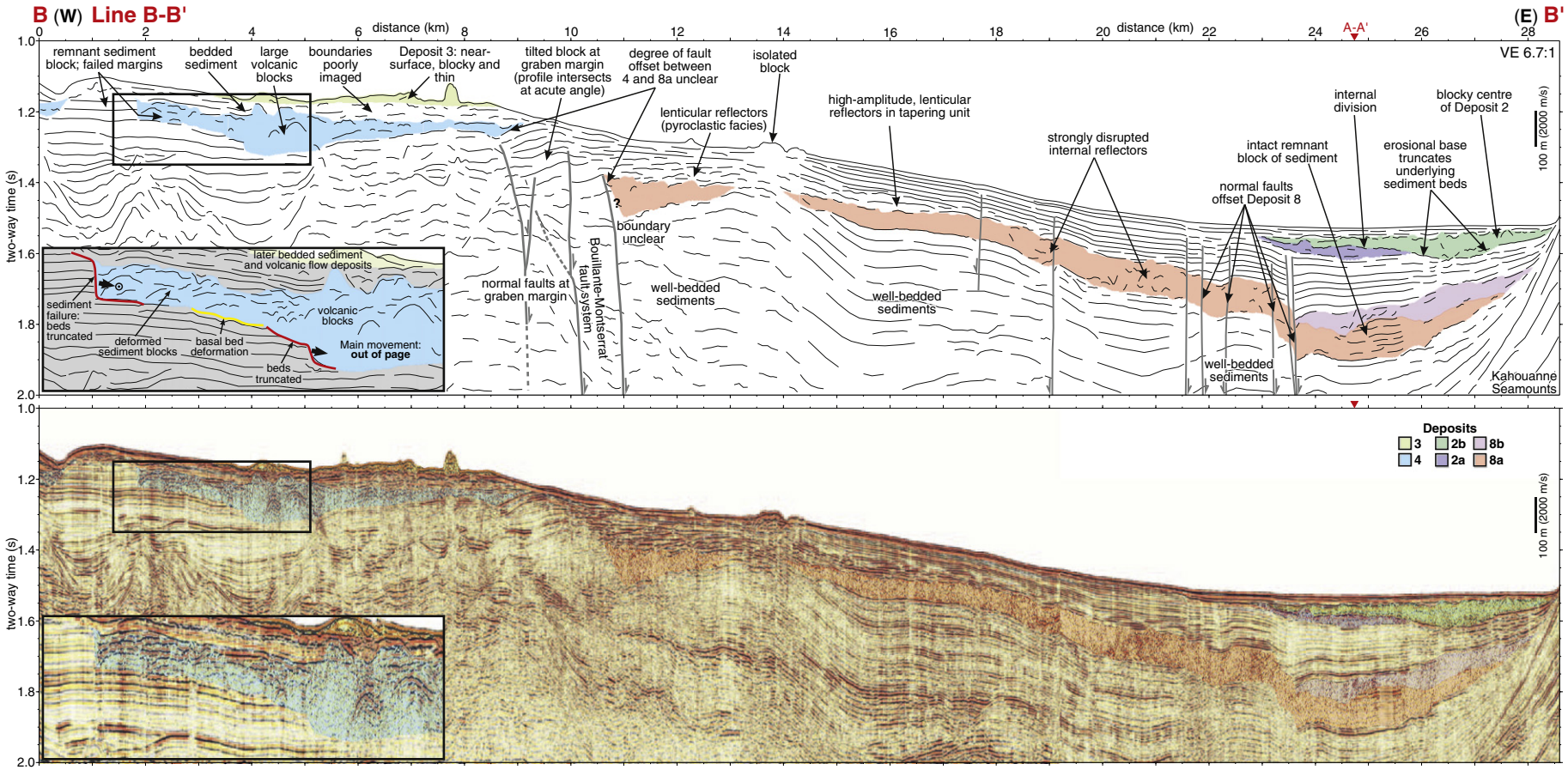

Fig. 7. Interpreted 2D seismic profile (air gun source) across the Bouillante-Montserrat Graben (location in Fig. 5), showing the landslide deposits discussed in the text.

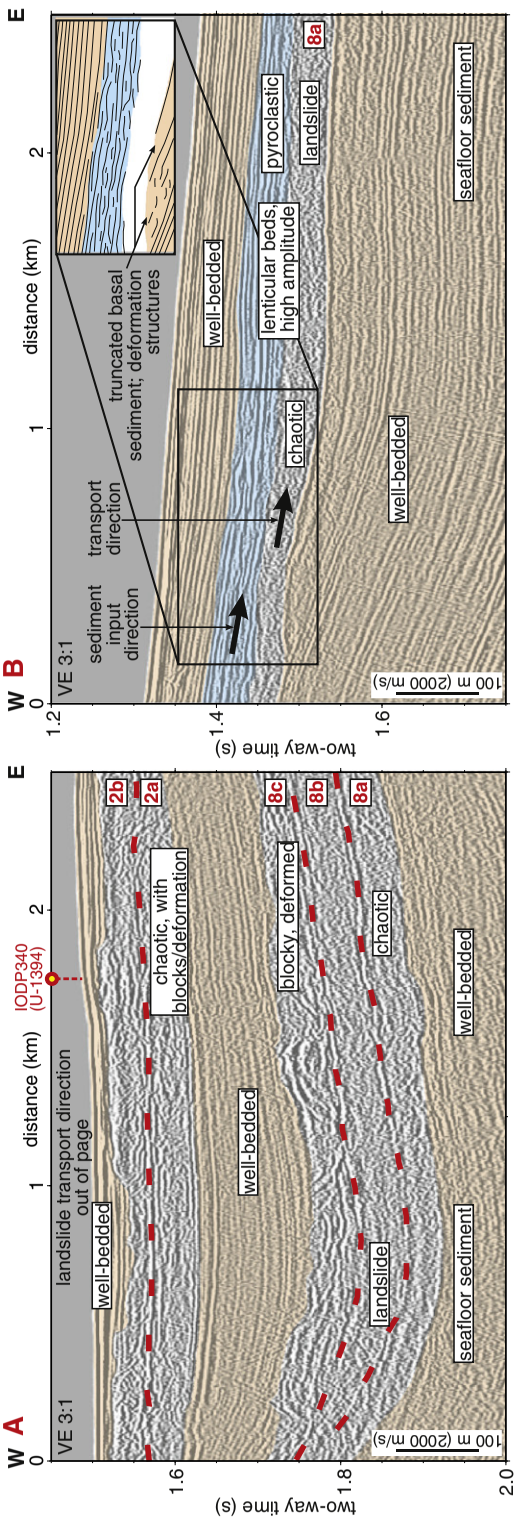

Fig. 8. Interpreted 2D seismic profiles (air gun source) showing the different appearance of the defined seismic facies (facies types shown in italics; line locations in Fig. 5). Individual landslide deposits are labelled, and an IODP 340 drill site is also indicated. Red dotted lines indicate internal boundaries within the landslide deposits. (For interpretation of the references to colour in this figure legend, the reader is referred to the web version of this article.)

Please cite this article as: Watt, S.F.L., et al., Widespread and progressive seafloor-sediment failure following volcanic debris avalanche emplacement: Landslide dynamics and timing offshore Montserrat,..., Marine Geology (2012), http://dx.doi.org/10.1016/j.margeo.2012.08.002

Please cite this article as: Watt, S.F.L., et al., Widespread and progressive seafloor-sediment failure following volcanic debris avalanche emplacement: Landslide dynamics and timing offshore Montserrat,..., Marine Geology (2012), http://dx.doi.org/10.1016/j.margeo.2012.08.002

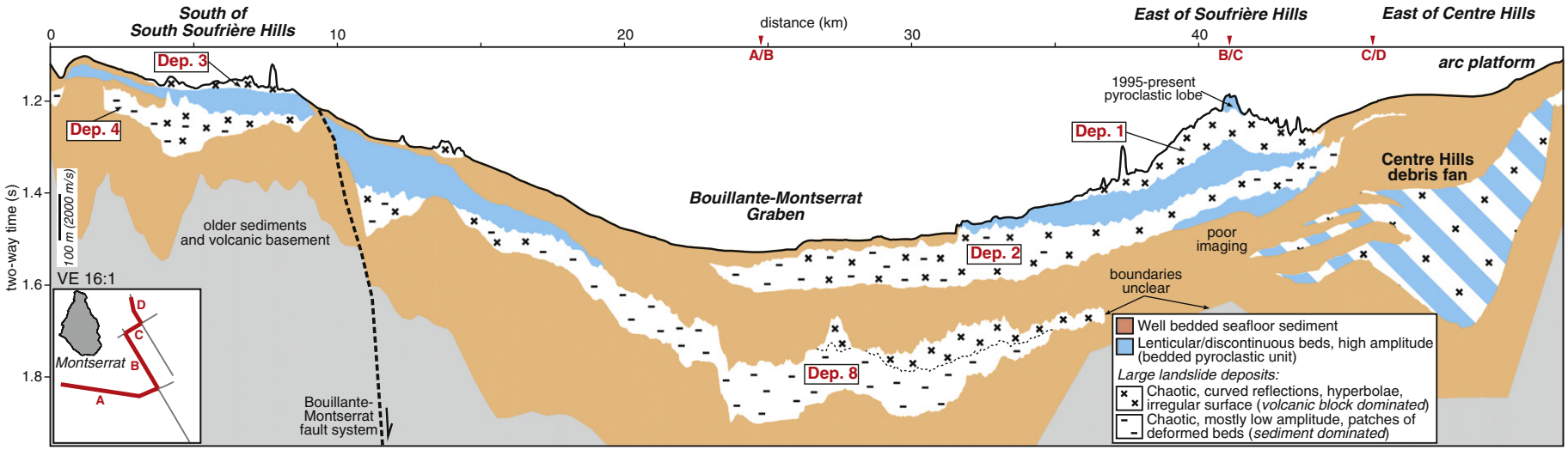

Fig. 9. Summary seismic facies profile around the SE sector offshore Montserrat (see inset map), distinguishing well-bedded seafloor sediment from pyroclastic deposits and large landslide deposits. An unconformity has been roughly picked below Deposit 8 (the base of the coloured sediment package) to highlight variable rates of overlying sediment accumulation. (For interpretation of the references to colour in this figure legend, the reader is referred to the web version of this article.)

ARTICLE IN PRESS

Deposit 8 exhibit low amplitudes and have little structure. Based on data presented below, we suggest that they are dominated by failed seafloor sediment. In contrast, the top sub-unit contains high-amplitude curved reflections, and we suggest it is dominated by volcanic blocks.

4.2. Stratigraphy and morphology of Deposit 2

A high amplitude internal reflection, traceable for 15 km down the western half of Deposit 2 (Figs. 6 to 8), defines Deposits 2a (lower) and 2b (upper) (Watt et al., 2012). In places, this bright reflection thickens to a discrete package of reflections, up to 20 m in thickness. In eastern and proximal areas, where Deposit 2b may have eroded Deposit 2a, the reflection is not clearly imaged. Based on our picked division, we obtain volumes of 3.2 km^3 for 2a and 6.3 km^3 for 2b (Table 1). This total volume of 9.5 km^3 is slightly larger than the 8.4 km^3 estimated by Lebas et al. (2011) (for 2000 m s^{-1} seismic velocity), due to slightly revised deposit outlines, particularly near the head of Deposit 2 (Section 4.5).

Deposits 2a and 2b have very similar seismic characteristics (Figs. 6 and 8) and similar elongate shapes (Fig. 10), although the basal reflection of Deposit 2b is stronger. Both sub-units contain rounded reflections more proximally, interpreted as volcanic blocks and correlating with a hummocky surface morphology (Fig. 3). Towards the deposit margins, a smooth surface is associated with a lower-amplitude, chaotic character. The two surface morphologies do not correspond to the division into Deposits 2a and 2b; both have a blocky centre surrounded by a smoother apron, with 2a largely buried beneath 2b.

4.3. Stratigraphy and morphology of Deposit 8

In the deepest part of the Bouillante-Montserrat Graben, Deposit 8 is separated from Deposit 2 by 200 m of well-bedded sediment (Fig. 7), and underlain by >300 m of bedded sediment. In this area, high-amplitude internal reflections divide Deposit 8 into three sub-units, 8a, 8b and 8c (Figs. 6 to 8). Deposit 8a extends along the NW arm of the Bouillante-Montserrat Graben, while 8b and 8c extend to the north. The three overlapping sub-units form a two-lobed deposit, and suggest more than one source region (Fig. 10). Folding and faulting have affected Deposit 8 (Fig. 6), and contemporaneous seafloor gradients cannot be measured. However, comparison with Deposit 2 and the current structure of the graben suggests that slopes were <1° in the distal parts of Deposit 8.

Deposit 8a is the thickest sub-unit (mean thickness of 60 m; Table 1), with a volume (11 km^3) larger than the whole of Deposit 2. The volumes of Deposits 8b and 8c are estimated at ≥3.2 and ≥2.0 km^3 respectively (Table 1), but we cannot map their proximal limits. Our total volume of >16.2 km^3 compares with 18.6 km^3 estimated by Lebas et al. (2011), and is explained by slight changes to defined deposit limits.

4.3.1. Deposit 8a

Deposit 8a, at the base of Deposit 8, has smooth upper and lower surfaces parallel with the underlying sedimentary bedding. There is no evidence for large volcanic blocks within the deposit. At its western margin, Deposit 8a abuts normal fault scarps of the Bouillante-Montserrat fault system (Fig. 10C). Because Deposit 8 follows the present shape of the Bouillante-Montserrat Graben, we suggest these faults were active and formed seafloor scarps when Deposit 8a was emplaced.

The western part of Deposit 8a is overlain by a unit of the pyroclastic facies, up to 100 m thick (Figs. 7 to 9). This unit tapers rapidly away from the island flanks, and is overlain by up to 75 m of seafloor sediment.

4.3.2. Deposit 8b

Deposit 8b has a similar low-amplitude seismic character to Deposit 8a, with no evidence for large volcanic blocks (Fig. 8). The sub-units are separated by a single high-amplitude but discontinuous reflection, which is more easily picked over most of the deposit than the internal division in Deposit 2. Deposit 8b has a relatively constant thickness of ~40 m where it overlies 8a (Fig. 10). The upslope limit of Deposit 8b extends into the northern part of the Bouillante-Montserrat Graben, where it is poorly imaged beneath Deposit 2.

4.3.3. Deposit 8c

Deposit 8c is dominated by high-amplitude, curved reflections (Figs. 6 and 8), suggesting the presence of large volcanic blocks, in contrast to the sub-units below. Isolated rounded blocks at the toe of Deposit 8c have comparable dimensions to those in Deposit 2, and its shape and run-out (Fig. 10; Table 1) is similar to the blocky part of Deposit 2. Deposit 8c extends into the northern part of the Bouillante-Montserrat Graben, and appears to have been sourced from a flank collapse on the eastern or south-eastern flank of Montserrat.

4.4. Seafloor-sediment incorporation in Deposits 2, 4 and 8

4.4.1. Sediment incorporation in Deposit 2

At the northern edge of Deposit 2, 50 m of seafloor-sediment beds are truncated (Fig. 11). These beds dip at 2° to the SW and trace stratigraphically into the base of Deposit 2, where deformed seismic

Table 1
Parameters of Deposits 2 and 8.

Unit	Area (km^2)	Volume (km^3)[a]		Max. thickness[b] (s twt) *(m)*[c]		Mean thickness (s twt) *(m)*[c]		Shore to toe distance[d] (km)	Toe depth[e] (s twt)	Estimated age (ka)
		2000 m s^{-1}	2150 m s^{-1}							
Deposit 2	212	9.5	10.3	0.141	*141*	0.045	*45*	34	1.60	~140
-2a	84	3.2	3.5	0.127	*127*	0.039	*39*	23	1.62	~140
-2b	181	6.3	6.8	0.127	*126*	0.035	*35*	34	1.60	~140
Deposit 8[f]	~250	>16	>17	0.178	*178*	0.066	*66*	30	1.79	~700
-8a	183	11.0	11.8	0.123	*123*	0.060	*60*	30	1.79	~700
-8b	~100	≥3.2	≥3.4	0.062	*62*	0.032	*32*	n/a[e]	1.83	~700
-8c	~60	≥2.0	≥2.2	0.090	*90*	0.034	*34*	23	1.75	~700

[a] The higher seismic velocity is used to allow comparison with Lebas et al. (2011). This velocity is suitable for deposits dominated by heterogeneous volcanic material. For Deposits 2 and 8, dominated by seafloor sediment, 2000 m s^{-1} is likely to provide more accurate volume estimates (cf. Paulatto et al., 2010).
[b] Excludes individual large blocks prominent above the seafloor (e.g., in Deposit 2).
[c] Assuming a seismic velocity of 2000 m s^{-1}.
[d] Measured from modern shoreline along assumed transport path.
[e] Depth of basal surface below sea level at most distal point. This does not precisely reflect depth at time of deposition, due to subsequent sedimentation, faulting and folding.
[f] 8a assumed source from south of Centre Hills (potentially Deposit 4), and 8c from east of Centre Hills; 8b assumed to entirely comprise seafloor sediment.

Please cite this article as: Watt, S.F.L., et al., Widespread and progressive seafloor-sediment failure following volcanic debris avalanche emplacement: Landslide dynamics and timing offshore Montserrat,..., Marine Geology (2012), http://dx.doi.org/10.1016/j.margeo.2012.08.002

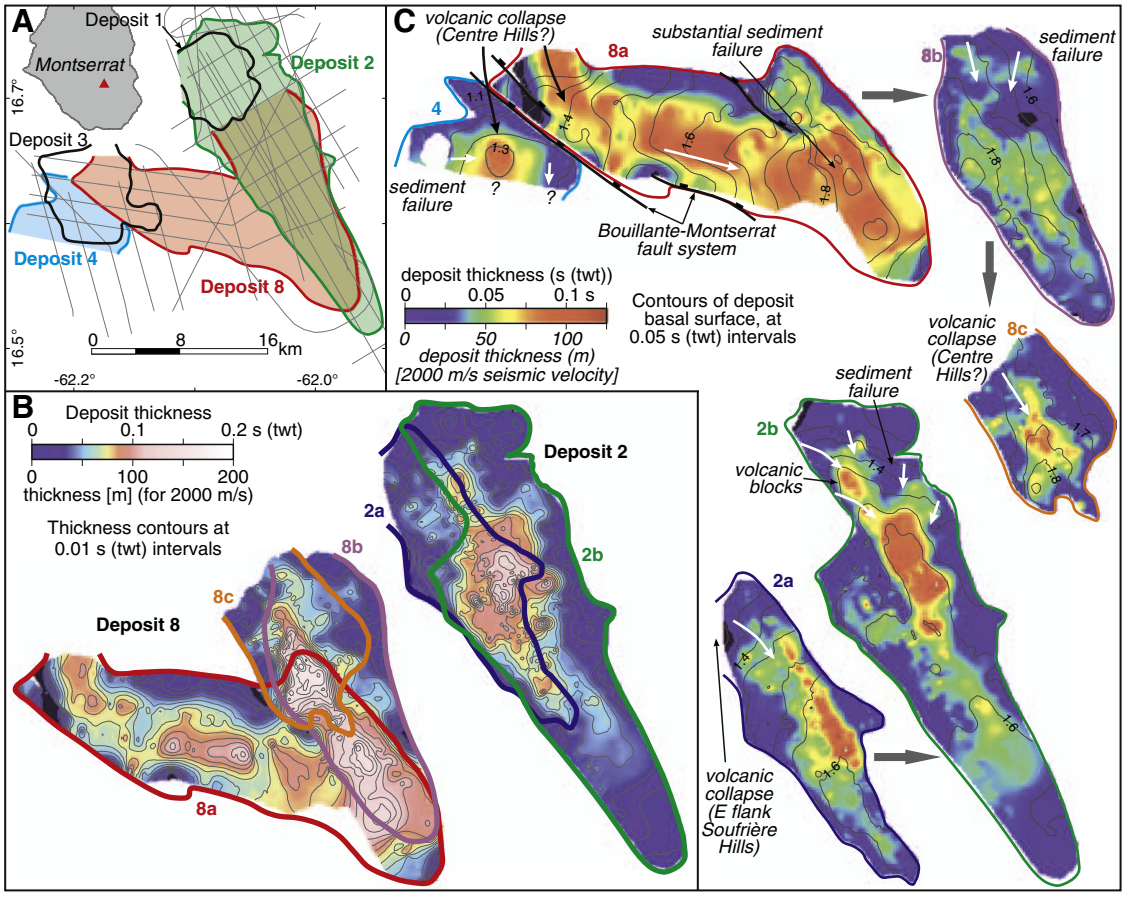

Fig. 10. A: outline map of the large landslide deposits discussed in the text. Grey lines show coverage of 2D seismic data. B: contoured and shaded isopach maps for the composite landslide Deposits 2 and 8, with the divided parts outlined. C: shaded isopach maps for all individual landslide deposits discussed in the text, showing contours of the basal deposit surfaces, labelled in two-way time. The grey arrows show the deposit age sequence, from the oldest unit to the youngest.

reflections indicate mixing of seafloor sediment and volcanic blocks. Proximally, debris avalanche emplacement therefore involved in-situ incorporation of the substrate, rather than the transportation of eroded sediment away from proximal areas.

Further east, the same truncated seafloor strata form an angular scarp (Fig. 4), which may exploit normal fault planes. South of the scarp, the pockmarked seafloor (Fig. 1) is interpreted as a disaggregated sediment slide transported along a basal decollement (Watt et al., 2012). Part of this slide material may have flowed down the graben, contributing to the tapering toe of Deposit 2b. To the south, truncated beds at the western margin of Deposit 2a and the eastern edge of Deposit 2b (Fig. 7) provide further evidence of seafloor-sediment incorporation.

Deposit 2a is 30 to 35 m thick at its toe and contains deformed parallel-bedded structures (Fig. 6). The deposit toe truncates parallel-bedded seafloor sediment, and shows no marginal accumulation above these beds. This toe structure is similar to that of Deposit 8a, which is better imaged. Deposit 2b runs out beyond 2a, and here contains deformed internal reflections (Fig. 6), which may represent rafted sediment blocks.

4.4.2. Bed truncation at the head of Deposit 4

At the western edge of Deposit 4, 50 m of seafloor sediment failed around a remnant block (Fig. 7) on a topographic high (Fig. 1). This western edge of Deposit 4 preserves deformed sedimentary bed structures, but does not contain large volcanic blocks. As in Deposit 2, much of the failed sediment was not transported away from this proximal area. Moving east and downslope, across the main transport direction of Deposit 4, deeper sediment beds are truncated, accounting for another 50 m of incision (Fig. 7). This central part of Deposit 4, containing large volcanic blocks, is accommodated in space previously occupied by seafloor sediment, now incorporated within the landslide deposit.

4.4.3. Sedimentary bed structures in Deposits 8a and 8b

Deposit 8a is transparent in the NW arm of the Bouillante-Montserrat Graben (Fig. 7), but internal bedding is abundant more distally (Figs. 12 and 13). Bed structures include in-situ remnant blocks with parallel bedding. The example in Fig. 12 is 1 km across (both N–S and E–W) and surrounded by structureless material. Elsewhere, internal beds are symmetrically folded (Fig. 13) with an amplitude that increases upwards, such that basal strata lie approximately parallel with the underlying sediment, and a wavelength of 500–1000 m. These structures extend downslope for > 10 km, and affect a consistent thickness of ~70 m.

Towards the toe of Deposit 8a, reverse faults and associated tight asymmetrical folds sharply abut parallel-bedded seafloor sediment (Fig. 13). The toe position is difficult to define precisely, but we pick it as the location where the strata have parallel bedding continuous with beds above and below. Some deformation has propagated beyond this point, forming symmetrical surface folds (Fig. 13).

Deposit 8b preserves lower levels of coherent structure than Deposit 8a, but still contains regions of folded beds that mimic the surface of the underlying Deposit 8a. In places, folds are tighter than in 8a, with a slight asymmetry towards the downslope side (Fig. 13).

Please cite this article as: Watt, S.F.L., et al., Widespread and progressive seafloor-sediment failure following volcanic debris avalanche emplacement: Landslide dynamics and timing offshore Montserrat,..., Marine Geology (2012), http://dx.doi.org/10.1016/j.margeo.2012.08.002

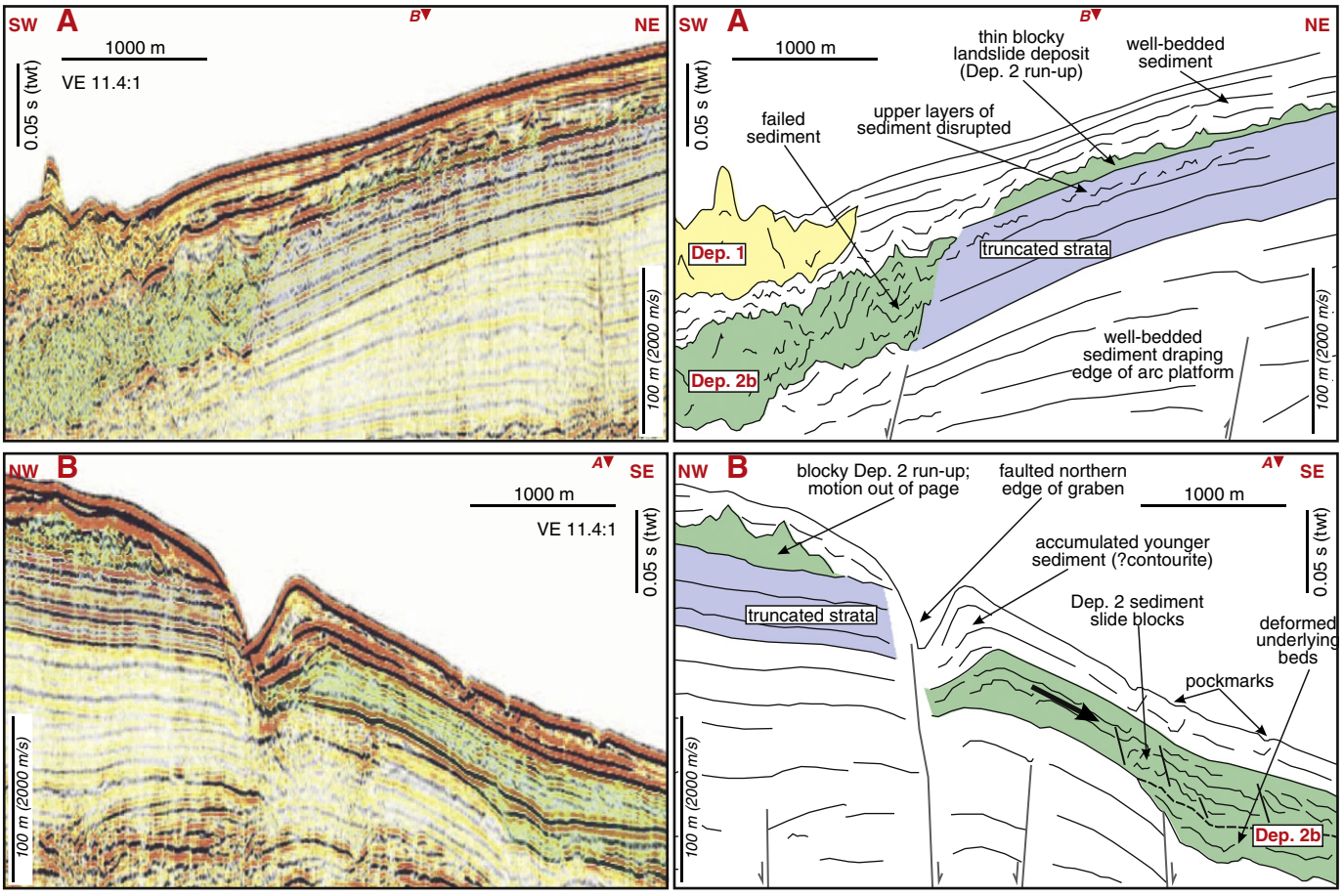

Fig. 11. Interpreted 2D seismic profiles (air gun source) showing structures around the sedimentary headwall of Deposit 2b. Bedded seafloor sediment failed in this region to form part of Deposit 2, and the equivalent (unfailed) stratigraphy is highlighted as truncated strata. The thin deposit overlying these strata is interpreted as a part of Deposit 2 that ran up onto the arc platform, at the same time as the underlying sedimentary beds failed and became incorporated into the landslide. Line locations in Fig. 5.

4.5. Run-up of Deposit 2

In contrast to Deposits 1, 3 and 4, which followed downslope trajectories, a northern limb of Deposit 2 ran up onto the arc platform and can be used to estimate landslide velocity (e.g., Pierson, 1985). The map in Fig. 14 shows the pre-Deposit 2 seafloor, approximated from seismic profiles. The northern limb of Deposit 2 was transported from the west onto a southward dipping slope. It has an irregular, blocky surface (Fig. 14), and we interpret it as the edge of a volcanic debris avalanche deposit (association with 2a or

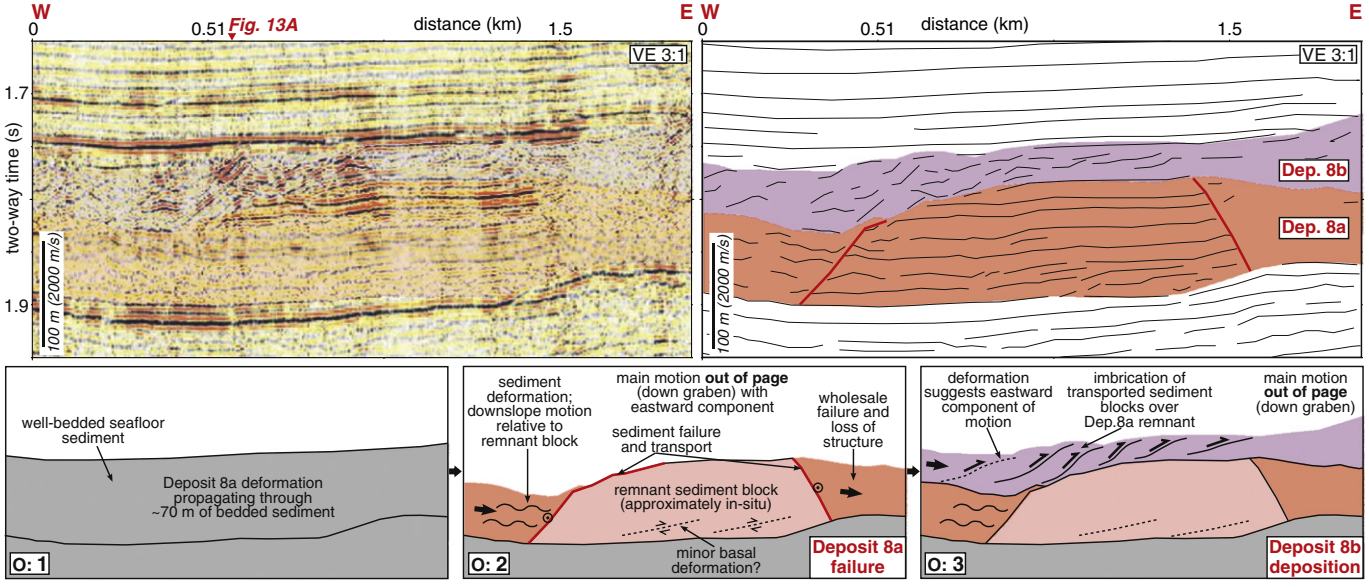

Fig. 12. Seismic profile and an interpreted deposition sequence (bottom) for a remnant block and surrounding deformed sediment in Deposit 8. Line location in Fig. 5.

ARTICLE IN PRESS

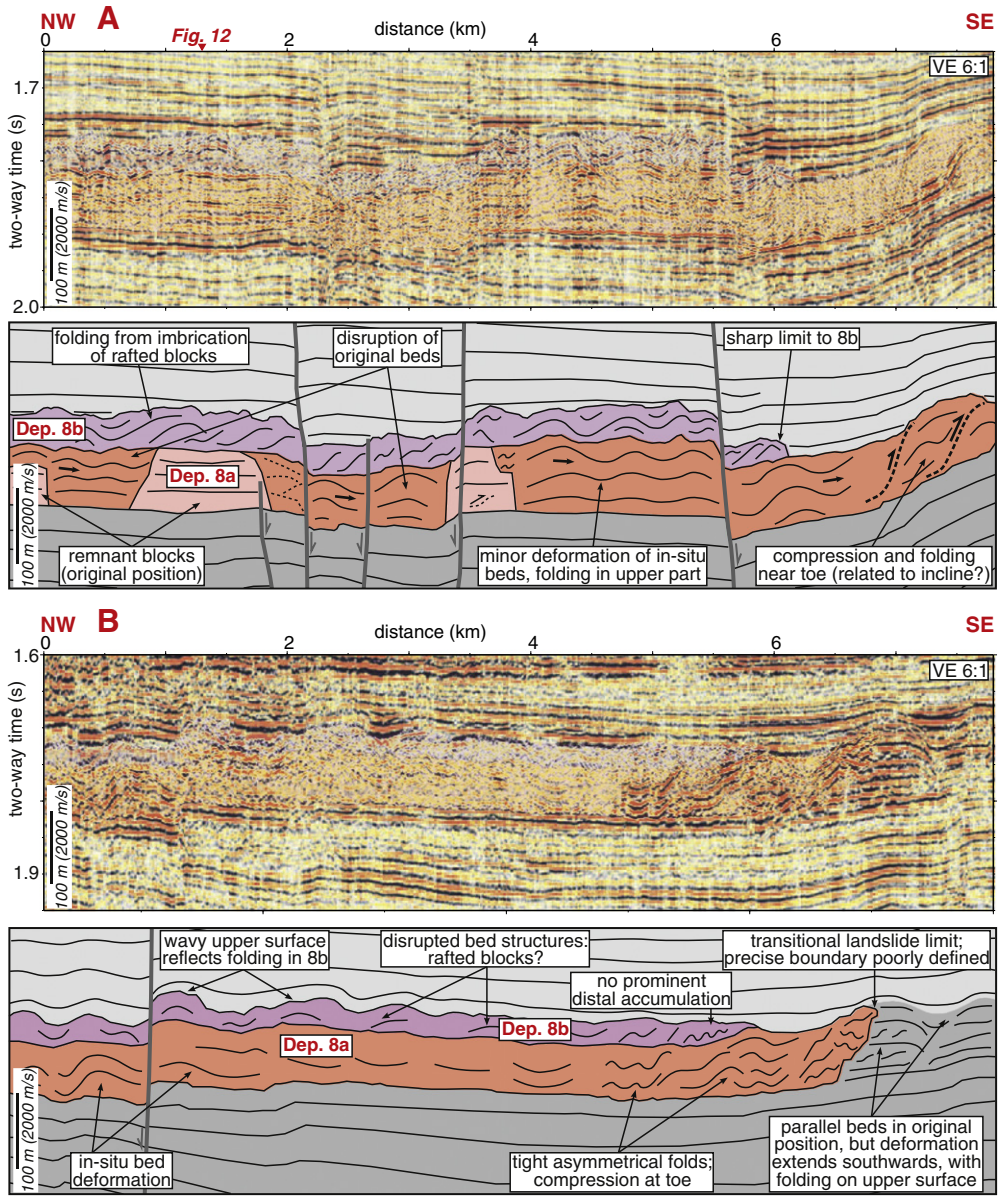

Fig. 13. Seismic profiles and interpretations showing sedimentary and deformation structures in the distal part of Deposit 8. Line locations in Fig. 5.

2b cannot be distinguished) which, unlike the bulk of Deposit 2's volcaniclastic component, did not enter the Bouillante-Montserrat Graben.

We estimate debris avalanche velocity at the base of a path indicated by the northernmost arrow on the map in Fig. 14, from the conversion of kinetic to gravitational potential energy (velocity $v=(2gh)^{0.5}$, where h is elevation gain and g is gravitational acceleration; Pierson, 1985). This assumes perpendicular collision and neglects frictional energy losses, thus providing a minimum velocity estimate. However, because landslide thickness is not accounted for, the elevation gain may be over-estimated, since material deposited on the arc platform did not necessarily climb from the base of the transport path (1.36 up to 1.21 s two-way-time). Our velocity estimate of 52 m s^{-1} is slightly lower than maximum velocities for subaerial volcanic debris avalanches (~70 m s^{-1} for Mount St. Helens 1980; Voight et al., 1983), and comparable to submarine velocity estimates (40 m s^{-1}, or possibly up to 80 m s^{-1}, based on tsunami observations following the Ritter Island 1888 collapse; Ward and Day, 2003).

The equivalent basal surface of Deposit 2 is associated with a prominent package of reflections that can be traced for several kilometres upslope on the arc platform (chirp SBP profiles in Fig. 14). This package may represent a widespread turbidite deposit associated with Deposit 2 (cf. Trofimovs et al., 2006). The unit lies 10–13 m below seafloor, and is ~2 m thick at a distance of 15 km north onto the arc platform.

5. Sub-unit relationships in Deposits 2, 4 and 8

5.1. Internal divisions in Deposits 2 and 8

The single, high-amplitude reflection between Deposits 8a and 8b does not necessarily imply a time gap between sub-unit emplacement; the material above and below may have moved synchronously. In contrast, the interval between Deposits 2a and 2b forms a discrete sedimentary unit, up to 20 m thick, whose nature remains unclear. At background sedimentation rates (see Section 7.2), this interval would take ~50 ka to accumulate. However, we suggest that the interval was

Please cite this article as: Watt, S.F.L., et al., Widespread and progressive seafloor-sediment failure following volcanic debris avalanche emplacement: Landslide dynamics and timing offshore Montserrat,..., Marine Geology (2012), http://dx.doi.org/10.1016/j.margeo.2012.08.002

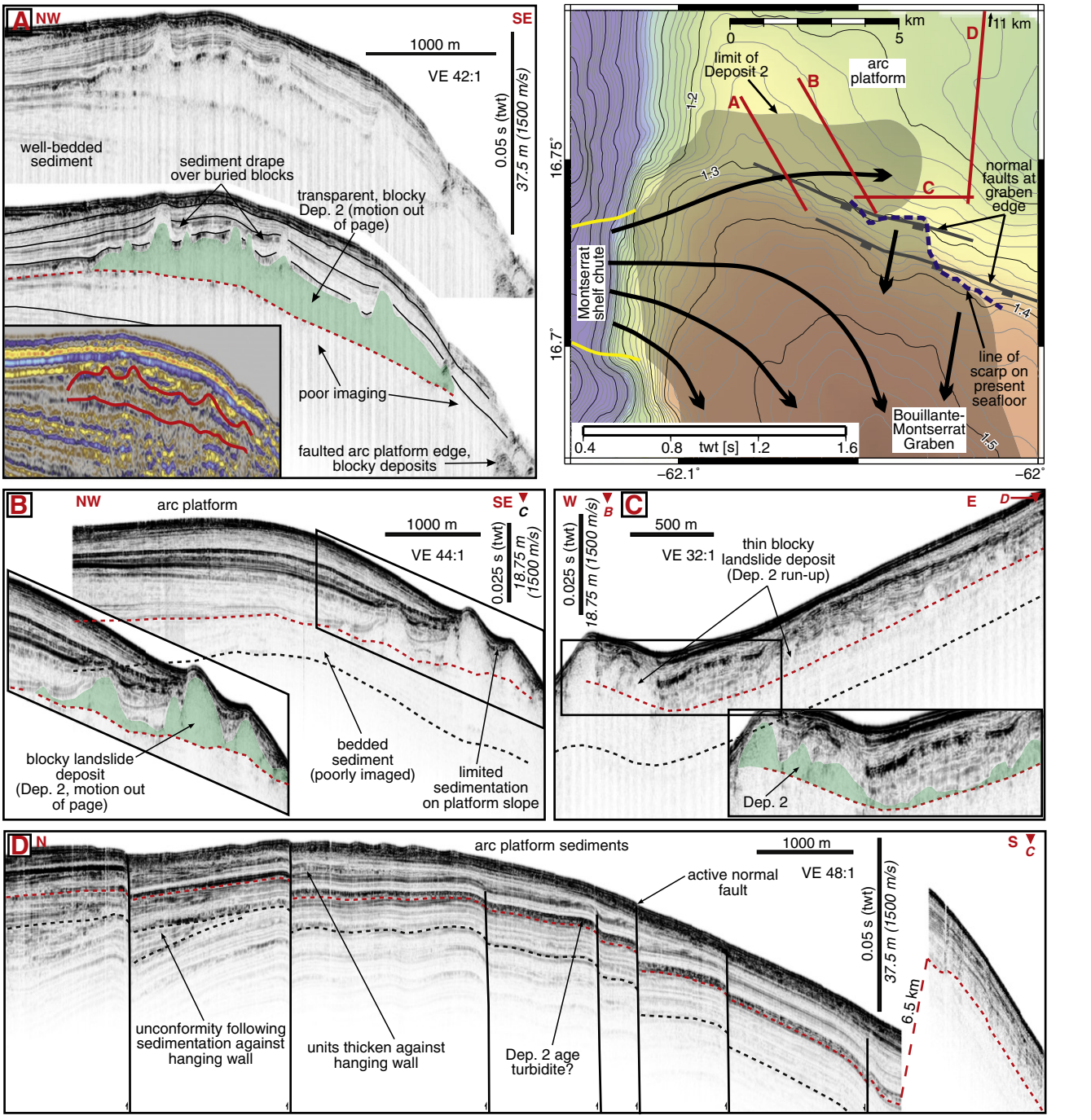

Fig. 14. Interpreted chirp sub-bottom profiler images from locations around the arc platform and the head of Deposit 2. Profile locations are shown in the map. The map show the pre-Deposit 2 seafloor (contoured in two-way time), based on the Deposit 2 basal surface picked from seismic profiles (Fig. 5). The limit of Deposit 2 is indicated. In profiles A to C the limb of Deposit 2 is imaged as a thin, blocky unit. The equivalent 2D seismic image is shown in profile A. The red dotted line in the chirp profiles marks the interpreted basal surface of Deposit 2 and its associated turbidite, while black dotted lines highlight selected sedimentary horizons. (For interpretation of the references to colour in this figure legend, the reader is referred to the web version of this article.)

emplaced in a brief period of time, between two associated landslides. Thicker patches of the interval are isolated, and in general it is confined to the deeper, western part of the graben, indicating a topographically confined deposit. One possibility is that a fine-grained flow deposit was emplaced between the two stages of Deposit 2, either relating to volcanic activity or to a seafloor-sediment failure, and that this flow deposit in-filled the irregular upper surface of Deposit 2a.

5.2. Relationship of Deposits 4 and 8a

We cannot correlate Deposit 8a with the stratigraphy west of the Bouillante-Montserrat fault system (Fig. 7), due to the fault offset and a lack of crossing seismic lines. Deposit 4 lies immediately to the west (Le Friant et al., 2004; Lebas et al., 2011), and is over 100 m thick in parts, with evidence for large volcanic blocks in its centre (Fig. 7). We speculate that Deposits 4 and 8a represent the

Please cite this article as: Watt, S.F.L., et al., Widespread and progressive seafloor-sediment failure following volcanic debris avalanche emplacement: Landslide dynamics and timing offshore Montserrat,..., Marine Geology (2012), http://dx.doi.org/10.1016/j.margeo.2012.08.002

ARTICLE IN PRESS

same landslide. This is consistent with the spatial extent of each deposit and with their sediment cover, which is ~50 m over the western part of Deposit 8a (excluding the pyroclastic facies) and at the western edge of Deposit 4 (Fig. 7). Furthermore, the thickness of Deposit 8a in this region (60 m) is broadly consistent with the deep incision of seafloor sediment (up to 100 m) by Deposit 4. Deposit 4 provides a plausible volcanic debris avalanche trigger for Deposit 8a, which otherwise preserves no evidence of a blocky volcanic component.

5.3. Emplacement sequences

5.3.1. Deposit 2

The emplacement of Deposit 2 remains ambiguous. Although Deposits 2a and 2b have blocky centres with smooth margins, the most proximal part of Deposit 2 forms a coherent blocky deposit, with no clear internal division. Here, sediment bed truncations trace into the base of the deposit, but further east the same truncations form a scarp that fed the tapering toe of Deposit 2b. These proximal observations suggest that the emplacement of volcanic blocks and sediment failure occurred together initially, with sediment sliding then continuing from the NE headwall. Apparently contradicting this, the interval between Deposits 2a and 2b suggests two discrete landslide stages, with both involving blocky volcanic material and seafloor sediment.

We suggest that the most likely model involved two stages of volcanic flank collapse. For Deposit 2a, proximal incision into seafloor sediment occurred, as well as deformation of in-situ sediment beyond the volcanic deposit margins. Deposit 2b may then have involved further volcanic failure, perhaps with proximal remobilisation or erosion of the underlying Deposit 2a, and caused additional failure to the east of the strata already incised by Deposit 2a.

5.3.2. Deposits 4 and 8

We suggest that loading and incision of seafloor sediment following emplacement of a volcanic debris avalanche (Deposit 4) triggered failure that propagated to the east as Deposit 8a. Deposit 8a appears to entirely comprise seafloor sediment, except perhaps in its more proximal part, where our imaging is poor. We suggest that Deposit 8b also comprises seafloor sediment and that its emplacement was directly associated with Deposit 8a (Section 6). A direct relationship between Deposits 4, 8a and 8b implies a landslide covering >300 km^2 and with a volume of at least 17 km^3 (using 3.2 km^3 for Deposit 4; Lebas et al., 2011), ~80% of which comprised seafloor sediment.

We interpret Deposit 8c as a volcanic debris avalanche emplaced after the other parts of Deposits 4 and 8. At its base, a patchy unit of irregular and high-amplitude reflections (10–20 m), observable towards its margins (Fig. 6), suggests a package of deformed intervening sediment. Without information on the nature of this sediment we cannot assess the time gap between Deposits 8b and 8c, but it is possible that Deposits 4 and 8c represent flank collapses associated with the same episode of volcanic activity.

6. Mechanisms of seafloor-sediment failure

Sediment failure in Deposit 8a propagated for tens of kilometres, on a seafloor gradient of $<1°$. Such low gradients would generally be well within the limits of stability in terrestrial settings, and failure is likely to require a process that increases pore pressure and reduces sediment shear strength. In this section, we discuss the formation and propagation of this type of marine landslide deposit.

6.1. Triggering and extent of sediment failure

The base of Deposit 8a follows a consistent stratigraphic horizon, whose depth may be determined by incision of a parental debris avalanche (Deposit 4) or may simply reflect the depth of the highest excess pore pressures. The lack of disruption in sediment (>300 m) bounding Deposit 8 suggests these strata are inherently stable, and that failure requires an external trigger. The fact that stratigraphic structure is so widely preserved through Deposit 8a suggests that the main landslide mass deformed by brittle or plastic deformation in response to stresses induced by movement on a weak basal failure plane. Structures are preserved more widely towards the deposit toe, suggesting that overall levels of disruption decreased downslope. However, the lack of topographic accumulation and consistent deposit thickness (Fig. 13) indicates minimal downslope transport across the landslide in general, and fits with the non-emergence (frontal confinement) of the landslide at the deposit toe (Fig. 13).

Although Deposit 8a has characteristics comparable to bedding-plane controlled landslides such as the Mauritania Slide (Masson et al., 2010), failure was not retrogressive and did not evacuate a source scar, but rather was driven progressively in a downslope direction, along the NW arm of the Bouillante-Montserrat Graben and then south into the deepest part of the graben. The extent of this gravitationally-driven deformation reflects both the initial debris avalanche energy and the seafloor topography. The deposit toe lies against an E–W striking uplifted fault block (Fig. 6). Several faults with this orientation cut Deposit 8 (Section 7), but we suggest this faulting also formed pre-existing seafloor topography, and that deformation was unable to propagate upslope against this (e.g., Trincardi and Argnani, 1990). A faulted offset of the basal shear plane may also have limited landslide propagation.

6.1.1. Controls on frontal confinement

A thick package of sediment deforming on low gradients may have insufficient energy to abandon basal shear surfaces and emerge onto the seafloor, and thus remains frontally confined (cf. Frey-Martínez et al., 2006; Moernaut and De Batist, 2011). In such cases, the deposit toe comprises deformed beds that abut their undeformed equivalent strata. Additionally, downslope transportation may only be significant in proximal areas; the major volume of the landslide is disturbed essentially in-situ (Lastras et al., 2004). For a landslide such as Deposit 8a, the term run-out is therefore defined as the distance between the deposit head and toe (Moernaut and De Batist, 2011), and does not correspond to the (insignificant) distance that individual particles have been transported.

Landslides comparable to Deposit 8a have been documented in a few non-volcanic settings (e.g., Trincardi and Argnani, 1990; Huvenne et al., 2002; Berndt et al., 2012), with initiation in some instances driven by upslope loading (Schnellman et al., 2005; Minisini et al., 2007). The presence of isolated remnant blocks (Fig. 12) may be a characteristic feature (Frey-Martínez et al., 2006). In general, frontal confinement may be favoured for landslides that are thick in comparison to their downslope width. In the case of sediment failure driven by volcanic debris avalanche emplacement, deep seafloor incision may provide the necessary conditions for destabilisation along a relatively deep decollement. Landslides similar to Deposit 8a may be common around volcanic islands, but due to their limited surface expression and because few such settings have been investigated with high-resolution seismic data, they have not been widely recognised.

6.1.2. The relationship between Deposits 8a and 8b

Structures within Deposit 8b are less extensive than in Deposit 8a, and suggest a greater amount of downslope transport. Over the remnant block in Fig. 12, we interpret asymmetrical folds in Deposit 8b as the imbrication of cohesive sediment moving over a topographic obstacle (Deposit 8a). Asymmetrical folded structures are widely preserved towards the toe of Deposit 8b. Here, it tapers to a limit slightly inside Deposit 8a, although in their most distal parts the division between the two sub-units is not always clear.

Please cite this article as: Watt, S.F.L., et al., Widespread and progressive seafloor-sediment failure following volcanic debris avalanche emplacement: Landslide dynamics and timing offshore Montserrat,..., Marine Geology (2012), http://dx.doi.org/10.1016/j.margeo.2012.08.002

Morphologically, the surface of Deposit 8b is comparable to that observed in remoulded seafloor sediments elsewhere (Prior et al., 1984; Minisini et al., 2007), but similar pressure-ridge structures can also form in more freely-spreading debris flow deposits (cf. Bull et al., 2009). Thus, surface morphology alone cannot be used to infer the style of landslide motion (cf. Tripsanas et al., 2008).

The boundary between Deposits 8a and 8b follows a consistent stratigraphic horizon, defining differential deformation between the sediment above and below. The nature of this boundary is important for understanding the formation of the two sub-units. If the boundary represents the contemporaneous seafloor, then Deposit 8b must have originated from outside the immediate depositional area, and its internal structures would therefore represent transported sediment blocks (Fig. 15). Alternatively, if the top of Deposit 8b represents the contemporaneous seafloor, then both sub-units would have formed approximately in-situ, with the boundary representing an internal shear surface with greater deformation above.

The extent of Deposit 8b, tracing into the north arm of the Bouillante-Montserrat Graben (Fig. 10), favours a source from outside the depositional area (the first hypothesis above). In such a model,

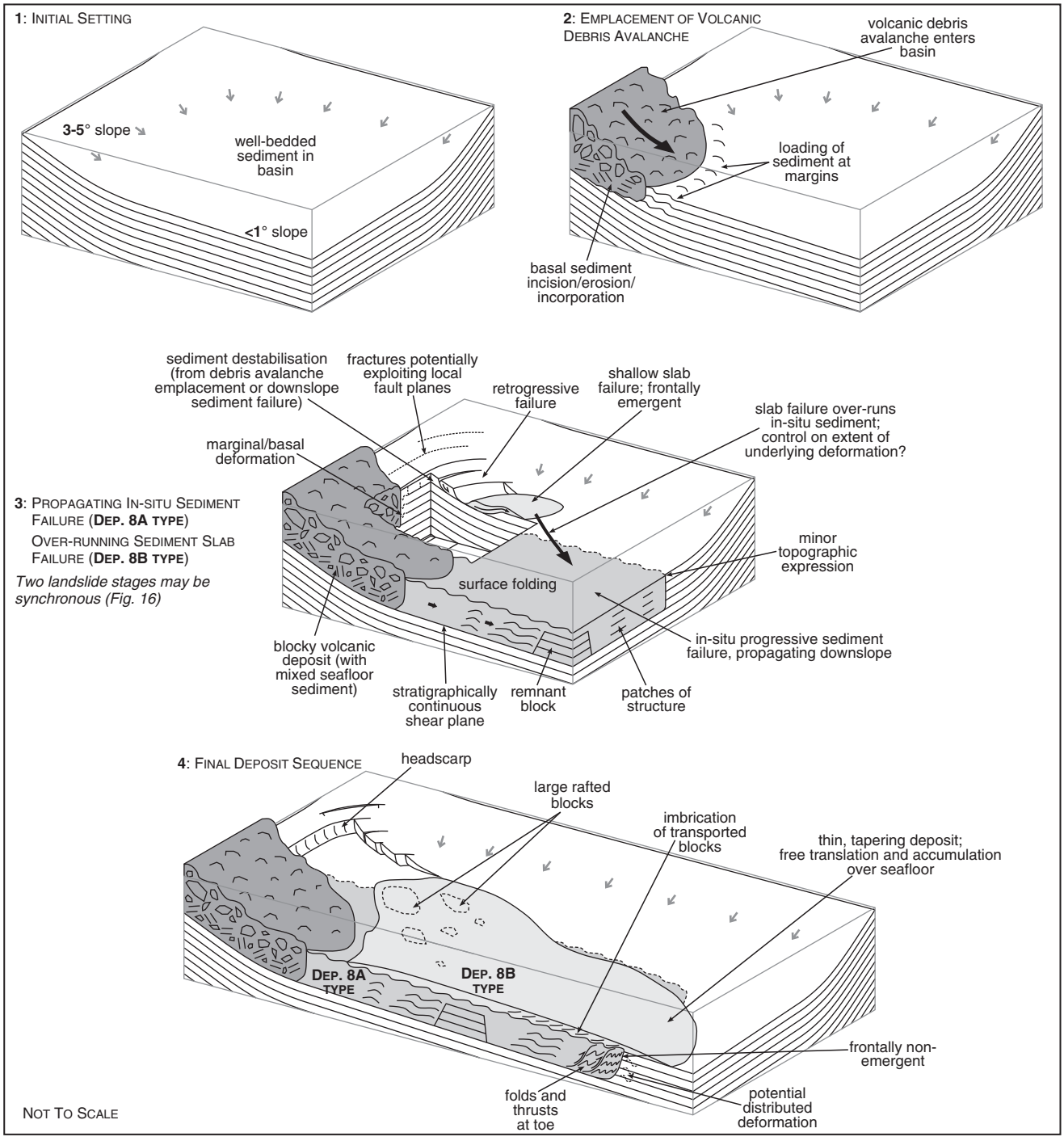

Fig. 15. Schematic illustration of the landslide failure sequence and dynamics discussed in the text. Emplacement of a volcanic debris avalanche on well-bedded seafloor sediment induces a downslope-propagating failure of in-situ sediment (Deposit 8a type), as a frontally non-emergent deposit. Resultant instabilities may induce further sediment slab failures, which are retrogressive and frontally emergent, translating freely across the seafloor as a tapering deposit (Deposit 8b type).

Please cite this article as: Watt, S.F.L., et al., Widespread and progressive seafloor-sediment failure following volcanic debris avalanche emplacement: Landslide dynamics and timing offshore Montserrat,..., Marine Geology (2012), http://dx.doi.org/10.1016/j.margeo.2012.08.002

ARTICLE IN PRESS

slide blocks could have failed retrogressively (from the north) in response to the downslope propagation of Deposit 8a, which entered the main graben from the west. However, we cannot entirely discount in-situ failure for Deposit 8b, since disruption of in-situ strata, driven from the west, may have propagated a little upslope to the north-west as well as moving south. Nevertheless, the lack of structure in the northern part of Deposit 8b, in contrast to its southern part, as well as the asymmetry of internal folding, suggests overall motion from north to south and argues against the latter model.

6.2. Models of sediment failure

Our interpretation suggests that Deposit 8a formed when a wave of progressive compressional deformation propagated through a consistent thickness of seafloor sediment for as long as the (deformation induced) mobilised shear stress exceeded the critical shear stress of the sediment. The precise mechanism that drove this propagation (Fig. 16), and how this relates to the emplacement of Deposit 8b, is less clear.

The model in Fig. 15 shows loading by a volcanic debris avalanche preceding Deposit-8a and -8b type failures. The long propagation distance of these failures (on gradients of <1°), their approximately corresponding toe positions, and their internal structures that correspond on either side of a separating surface, all suggest that the two sub-units may have formed synchronously. Here, we discuss a range of mechanisms that could explain the observed deposit relationships.

6.2.1. Loading of undrained seafloor

Rapid loading of seafloor sediment can lead to undrained conditions (cf. Lambe and Whitman, 1969), whereby pore water pressures increase, potentially reducing sediment shear strength and initiating sediment failure. Similarly, the propagation of sediment failure on low gradients may be explained by a moving surface load, maintaining undrained conditions in the underlying sediment package. This underlying package forms a weak boundary layer, reducing basal landslide shear resistance, enhancing landslide run-out, and forming a final deposit that incorporates the layer of over-ridden sediment (cf. Voight and Elsworth, 1997; Voight et al., 2011).

In Fig. 15, we depict the contemporaneous seafloor as the surface of Deposit 8a. We favour this as the most likely model, given the structures and extent of Deposit 8b. The alternative, where both sub-units represent in-situ sediment, involves failure driven by a self-loading mechanism.

6.2.1.1. Loading by over-running flow. Undrained sediment loading by an over-running flow may plausibly produce landslides with a long run-out on low seafloor gradients. This potentially explains the formation of Deposits 8a and 8b, with 8a representing a deformed layer of in-situ sediment, and 8b the over-running landslide (Fig. 16A). We consider Deposit 8b to comprise failed seafloor sediment, based on its internal structures, but the scenario is identical for over-running material derived directly from a volcanic collapse (cf. Voight and Elsworth, 1997). In this model, the toe positions of the over-running material and the deformed underlying sediment correspond, since sediment deformation proceeds for as long as the over-running material is moving.

In the NW arm of the Bouillante-Montserrat Graben, we did not observe an internal division (and therefore no over-running 8b-type flow unit) within Deposit 8. However, this could simply indicate that any over-running material was not depositional in this upslope area, or may reflect poor seismic imaging.

6.2.1.2. Self-loading driven propagation. Frontally confined sediment failures have been imaged where there is no evidence of an over-running deposit (Frey-Martínez et al., 2006; Morita et al., 2011; Berndt et al., 2012). In such cases, we suggest that deformation may propagate through a self-loading mechanism. Failure requires an initial trigger (e.g., loading by a volcanic debris avalanche) at the head of the deposit.

In this model, a discrete package of sediment deforms progressively, thereby loading the package immediately downslope, which then fails (Fig. 16B). If this mechanism described the formation of Deposits 8a and 8b, the surface of 8b would mark the contemporaneous seafloor, and an internal shear surface would be required to explain differentiation into two sub-units. In such a case, greater downslope movement of the upper strata (Deposit 8b; approaching frontal emergence), would load the underlying strata (Deposit 8a; remaining fully confined). This is consistent with structures at the toe of Deposit 8, where the degree of deformation between Deposits 8a and 8b does not appear to differ substantially (Fig. 13). However, the model does not fit with the extent of Deposit 8b, which should match exactly that of Deposit 8a (including in upslope areas). Furthermore, stepwise progressive loading is not consistent with the distributed plastic deformation (folding) in Deposit 8a (Fig. 13), which is easily explained by a model involving an over-running surface load. In the self-loading model, we would also expect brittle shear surfaces to separate folded packages with regular imbrication (Fig. 16B, inset; Morita et al., 2011). Moreover, appealing to the formation of an internal shear surface introduces unnecessary complexity to this model. The simple imbricate packages in Fig. 16B (inset) suggest a self-loading mechanism may operate in nature, but this mechanism does not clearly fit with the formation of Deposits 8a and 8b.

6.2.2. Shear coupling

Deformation of in-situ sediment by an over-running landslide has been postulated elsewhere (e.g., Schnellman et al., 2005; Van Der Merwe et al., 2011). However, in some instances deformation may arise through shear coupling, via forces exerted on the underlying sediment by motion of the over-running material, rather than loading-induced excess pore pressure.

Field relationships for palaeo-landslide deposits in the Karoo Basin, South Africa (Van Der Merwe et al., 2011) suggest a shear coupling mechanism (Fig. 16C, inset). This example has comparable dimensions to Deposits 8a and 8b: 80 m of underlying strata are overlain by a 50 m debrite on gradients of <0.1°. The toe exhibits frontally-confined fold and thrust structures like those in Deposit 8a. However, the two deposit sub-units are tightly folded together, with a strong sense of asymmetry in the direction of transport (Fig. 16C), and in contrast to the symmetrical folding and approximately planar boundary of the Deposit 8 sub-units. Furthermore, the long run-out of Deposit 8b, on low gradients, requires a low-friction basal surface. This is incompatible with shear-induced deformation of underlying sediment, which could not occur in the presence of a low-friction basal layer. Thus, shear coupling is unlikely to explain the formation of Deposits 8a and 8b.

6.2.3. Shear rupture propagation

A final mechanism that could explain progressive in-situ sediment failure is shear rupture propagation (Puzrin et al., 2004; Petley et al., 2005; Viesca and Rice, 2010) at the base of the failed strata. The mechanism has been proposed for bedding-plane controlled landslides, and does not require excess pore pressures to accumulate along the entire landslide length, which may be unrealistic. Rather, failure is initiated in a focussed region of excess pore pressure (e.g., beneath the emplaced debris avalanche), and then propagates along a localised band of intense shear (Puzrin et al., 2004). This shear band can be treated as a slipping fracture, with much lower levels of plastic deformation characterising the overlying material (Fig. 16D). Normal surface stress changes, such as those due to avalanche loading, promote fracture propagation in a downslope direction (Viesca and Rice, 2010).

The shear rupture mechanism explains low-angle failure along a consistent basal plane within stable sediment, initiated by loading

Please cite this article as: Watt, S.F.L., et al., Widespread and progressive seafloor-sediment failure following volcanic debris avalanche emplacement: Landslide dynamics and timing offshore Montserrat,..., Marine Geology (2012), http://dx.doi.org/10.1016/j.margeo.2012.08.002

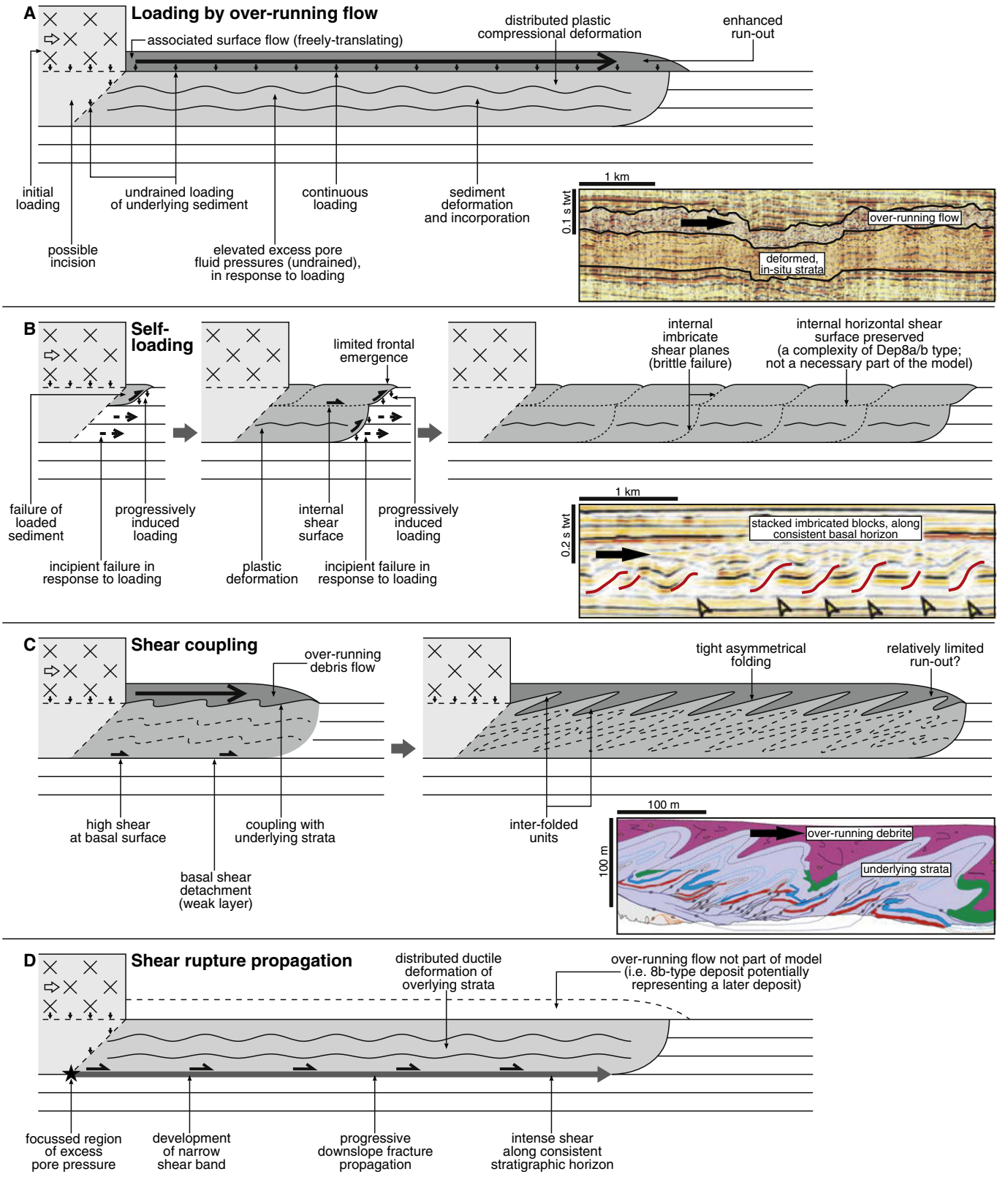

Fig. 16. Cartoons depicting mechanisms of progressively-driven seafloor-sediment failure. A and B show undrained sediment loading models (over-running flow and self-loading), C shows a shear coupling model, and D a shear rupture propagation model. The inset images for mechanisms A to C show possible examples of each. The inset for A is from Fig. 13, and we suggest that this is the most likely mechanism forming Deposits 8a and 8b (B or D are alternative potential mechanisms). The inset for B is from the continental slope off the Shimokita peninsula, NE Japan (Morita et al., 2011), while that for C is from the Vischkuil Formation (Rietfontein section) in the Karoo Basin (Van Der Merwe et al., 2011).

and producing a landslide where sedimentary structures remain largely intact. The mechanism is not mutually exclusive from those described above (Fig. 16A–C), since it concerns movement along the basal landslide plane, and could operate in conjunction with surface loading or shear processes that drive progressive sediment failure, potentially enhancing overall landslide run-out.

Please cite this article as: Watt, S.F.L., et al., Widespread and progressive seafloor-sediment failure following volcanic debris avalanche emplacement: Landslide dynamics and timing offshore Montserrat,..., Marine Geology (2012), http://dx.doi.org/10.1016/j.margeo.2012.08.002

ARTICLE IN PRESS

6.3. Comparison with examples elsewhere

The incorporation of thick packages of in-situ stratigraphy may be more common in the formation of submarine landslide deposits than is currently recognised. High-resolution seismic imaging from non-volcanic settings has revealed several cases where deposits with a comparable morphology to Deposit 8a are rich in internal structure (Schnellman et al., 2005; Frey-Martínez et al., 2006; Minisini et al., 2007; Bull et al., 2009; Morita et al., 2011), which may not be observable in lower resolution data. Thus, in seismic data, chaotic intervals do not necessarily represent extensively disaggregated or deformed material, transported over long distances (cf. Gafeira et al., 2010).

Frontally confined landslide deposits, similar to Deposit 8a, occur off Martinique and St. Lucia in the Lesser Antilles (Fig. 1). Their marginal sediment-bed truncations are 125 m and 150 m respectively (Deplus et al., 2001; Le Friant et al., 2003), compared with 70 m for Deposit 8a. Such sediment failure thicknesses are larger than the mean thickness of many non-volcanic submarine landslide deposits, including the Storegga Slide (mean thickness of 60 m; Canals et al., 2004; Hühnerbach and Masson, 2004). For the Martinique and St. Lucia deposits, deformation of sediment via an over-running flow has also been postulated (Deplus et al., 2001; Le Friant et al., 2003), and in both cases, a thin, tapering deposit (the 'bevel' in Le Friant et al., 2003) runs out at the deposit margins a little beyond the underlying sub-vertical truncations of seafloor sediment. We suggest these tapering deposits are the equivalent of Deposit 8b; they may either comprise failed seafloor sediment or fine-grained volcaniclastic material derived from a parental debris avalanche. Thus, there may be multiple instances of Deposit-8 type landslides, driven by an over-running flow, in the Lesser Antilles arc alone.

Total volumes of some volcanic-island landslide deposits are also consistent with substantial incorporation of seafloor sediment. For example, Le Friant et al. (2002) estimate that the largest flank collapse at Dominica (Fig. 1) had a volume of 18 to 20 km^3. This volume would provide a 7-m thickness over the associated landslide deposit area (3500 km^3; Le Friant et al., 2002), but seismic profiles show the deposit is an order of magnitude thicker.

6.4. Sediment incorporation as a control on volcanic debris avalanche mobility

The blocky region of Deposit 2 is elongate in comparison with the sub-circular Deposits 1 and 3 (Fig. 1), even though all these landslides experienced little topographic confinement. A sub-circular form is typical of many volcanic debris avalanche deposits in both subaerial and submarine settings (e.g., Siebert, 1984; Satake and Kato, 2001; Masson et al., 2002; Shea et al., 2008), and reflects transport dominated by solid grain forces in a low-cohesion, granular mixture, where energy is dissipated mainly through inter-grain impacts (Mulder and Cochonat, 1996; Iverson, 1997; Masson et al., 2002, 2006). More elongate deposits indicate relatively mobile debris avalanches with elements of cohesive flow (Naranjo and Francis, 1987; Stoopes and Sheridan, 1992; Richards and Villeneuve, 2001) and may contain linear longitudinal structures (Masson et al., 2006; Dufresne and Davies, 2009).

The high mobility of volcanic debris avalanches in general has been attributed to factors including intensive fragmentation, elevated hydrothermal fluid content, a high clay content or proportion of altered rock, the presence of low density grains, or the incorporation of water-saturated sediment (e.g., Voight et al., 1983; Crandell et al., 1984; Naranjo and Francis, 1987; Siebert et al., 1987; Vallance and Scott, 1997; Davies et al., 1999; Clavero et al., 2002). The nature of the substrate may play a particularly important role in determining mobility and shape, with water-saturated sediment potentially focussing shear in a weak basal layer, or rapid incorporation of this sediment reducing mean clast size and increasing fluid content. Both of these enhance mobility (Crandell et al., 1984; Legros, 2002; Hungr and Evans, 2004; Dufresne and Davies, 2009; Mangeney et al., 2010) and could produce more elongate deposits, potentially explaining the shape of the blocky part of Deposit 2 (Fig. 10).

Sediment incorporation occurred in Deposit 2 because it was emplaced on a substrate of poorly-consolidated seafloor sediment. The relatively elongate Deposit 8c was emplaced on a similar substrate (mostly the failed sediment of Deposit 8b). In contrast, the substrate for Deposits 1 and 3 was a thick sequence of pyroclastic deposits (pyroclastic facies, Fig. 9), likely to be coarser grained and heterogeneous and lacking laterally-continuous bedding. Emplacement of volcanic debris avalanches on saturated sediment is far more likely in the marine environment than in terrestrial settings. However, Parinacota in Chile (Clavero et al., 2002) provides a potential subaerial analogue for submarine volcanic debris avalanches with a long run-out. At Parinacota, emplacement on unconsolidated, well-bedded and saturated lake sediment, accommodated basal shear and led to enhanced spreading of the blocky volcanic material.

7. Landslide timing and volcanism on Montserrat

In this section, we estimate long-term sedimentation rates and assess the relationship between marine volcaniclastic sedimentation and the evolution of Montserrat.

7.1. Landslide deposits offshore Centre Hills

North of Deposits 1 and 2, a buried volcaniclastic fan lies offshore from Centre Hills (Kenedi et al., 2010) (Fig. 9). The fan is characterised by relatively high-amplitude, discontinuous curved reflections, with areas of more coherent bedding (Fig. 17), and is likely to comprise both pyroclastic-flow and flank-collapse deposits (e.g., Deposit 9 of Lebas et al., 2011). The sharp upper and lower surfaces of the fan suggest a discrete period during which volcaniclastic inputs dominated offshore sedimentation. The fan is overlain by up to 200 m of well-bedded and undisrupted sediments, and similar sediments lie below. We assume that the full thickness of the fan represents the period of active volcanism at Centre Hills. Equivalent horizons to the upper and basal surfaces of the fan can be traced across the study area, defining a sediment stratigraphy of Centre-Hills age, which we name the CH-unit.

The CH-unit encloses Deposit 8 (Fig. 17), confirming that it is associated with collapses of Centre Hills (i.e. it is of pre-Soufrière Hills age; cf. Lebas et al., 2011). This conclusion is consistent with the age of an uplifted submarine block at Roche's Bluff, on the south side of the Tar River Valley (Fig. 18), which is far older than the adjacent Soufrière Hills (~1020 ka) and was interpreted by Harford et al. (2002) as part of a debris fan south of Centre Hills. Deposit 4 and the pyroclastic facies overlying Deposit 8a (Fig. 9) may form part of this volcaniclastic fan, whose more proximal parts would now be buried beneath the South Soufrière Hills–Soufrière Hills complex.

The shape of the CH-unit basal surface (inset in Fig. 18) shows that the fan east of Centre Hills fills a small basin, north of the main Bouillante-Montserrat Graben, bounded by ENE–WSW striking faults on its south side. Faults with the same orientation cut across Deposit 8 further south (Figs. 6, 17–19), but have no surface expression on the modern seafloor. This contrasts with the graben faults (Fig. 19), which we suggest are younger overall. The latter strike NW–SE, or slightly oblique to the arc (Feuillet et al., 2010). Fault systems similar to the older, buried faults are well developed in the modern fore-arc (Feuillet et al., 2002, 2010; Kenedi et al., 2010), accommodating trench-parallel extension due to the curved geometry of the plate boundary.

Please cite this article as: Watt, S.F.L., et al., Widespread and progressive seafloor-sediment failure following volcanic debris avalanche emplacement: Landslide dynamics and timing offshore Montserrat,..., Marine Geology (2012), http://dx.doi.org/10.1016/j.margeo.2012.08.002

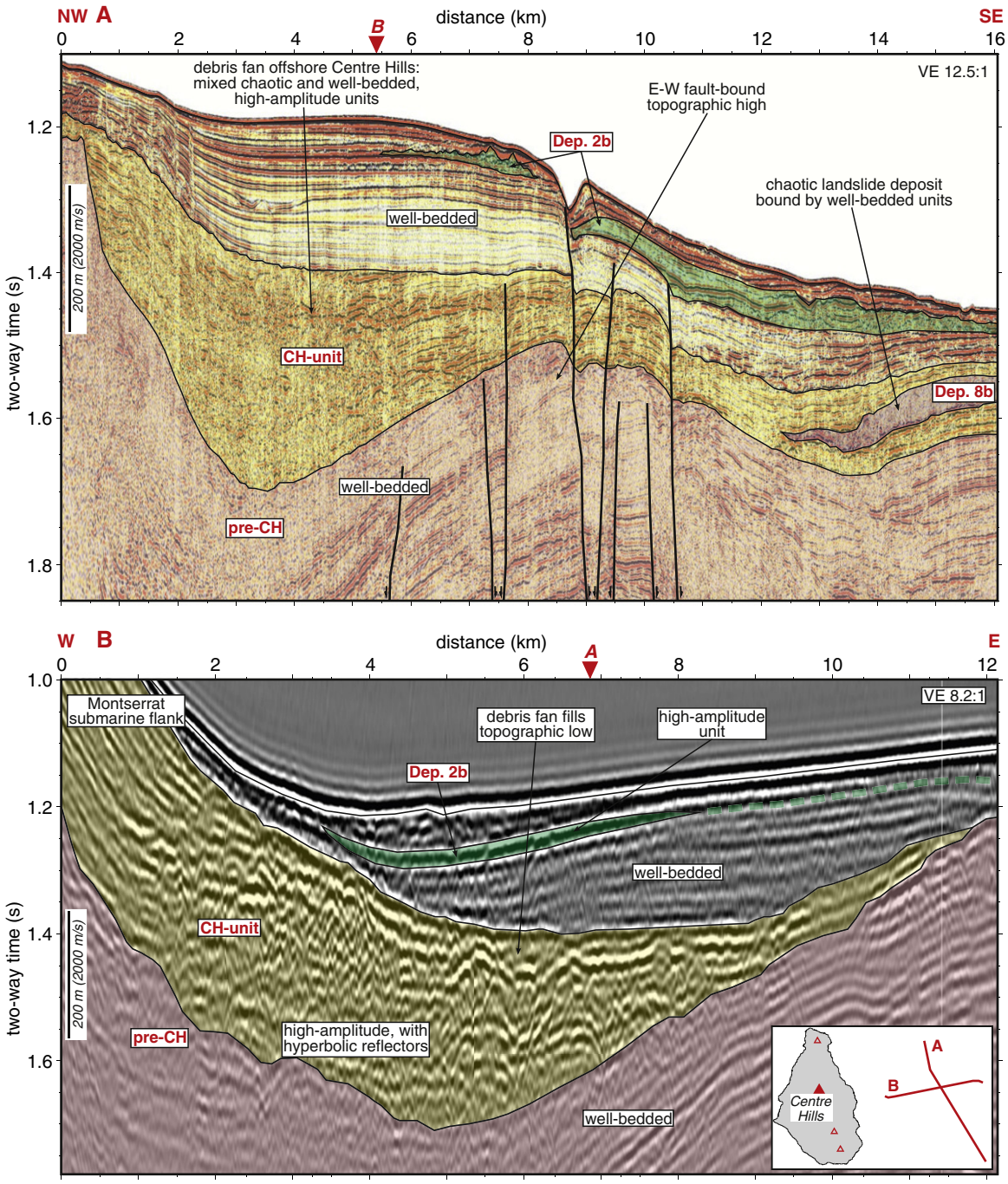

Fig. 17. Interpreted seismic profiles (top, from JC45/46; bottom, from SEA-CALIPSO (Kenedi et al., 2010)) showing the debris fan offshore from Centre Hills (CH-unit) and its relationship with landslide deposits discussed in the text. Line locations in Fig. 5.

7.2. Rates of sediment accumulation

To estimate sediment accumulation rates, we correlate the subaerial dates of Centre Hills volcanism (950–550 ka; Harford et al., 2002) with the CH-unit surfaces. The earliest Centre Hills rocks may not have been sampled or dated, and the basal surface age is likely to be slightly too young (for example, compare with the older Roche's Bluff date), leading to slightly over-estimated sedimentation rates. Assuming that the CH-unit represents a 400 ka time period, the thickest part of the Centre Hills debris fan (320 m) defines an average accumulation rate of 0.79 m ka^{-1}. The thickest overlying seafloor sediment (210 m) suggests an accumulation rate of 0.38 m ka^{-1}. Thus, sedimentation rates at this proximal offshore site approximately doubled during the period of active volcanism. Further offshore, the thickest sediment sequences in the Bouillante-Montserrat Graben define a sedimentation rate of 0.53 m ka^{-1}.

Outside the deep part of the Bouillante-Montserrat Graben, sediment accumulation rates (calculated from the base of the CH-unit to the present seafloor) are far lower. On the western arm of the graben, the rate is ~0.25 m ka^{-1}. On the more elevated arc platform, just 8 km east of the thickest part of the Centre Hills debris fan, the well-bedded sediment (50 m) defines a rate of 0.05 m ka^{-1}. Variations in topography and localised volcaniclastic inputs have therefore led to order-of-magnitude variations in sedimentation rates over distances of a few kilometres.

Our estimated sedimentation rate for the arc platform (0.05 m ka^{-1}) compares well with results using a similar method by Kenedi et al. (2010) (0.08–0.09 m ka^{-1}), and is consistent with dated shallow sediment cores

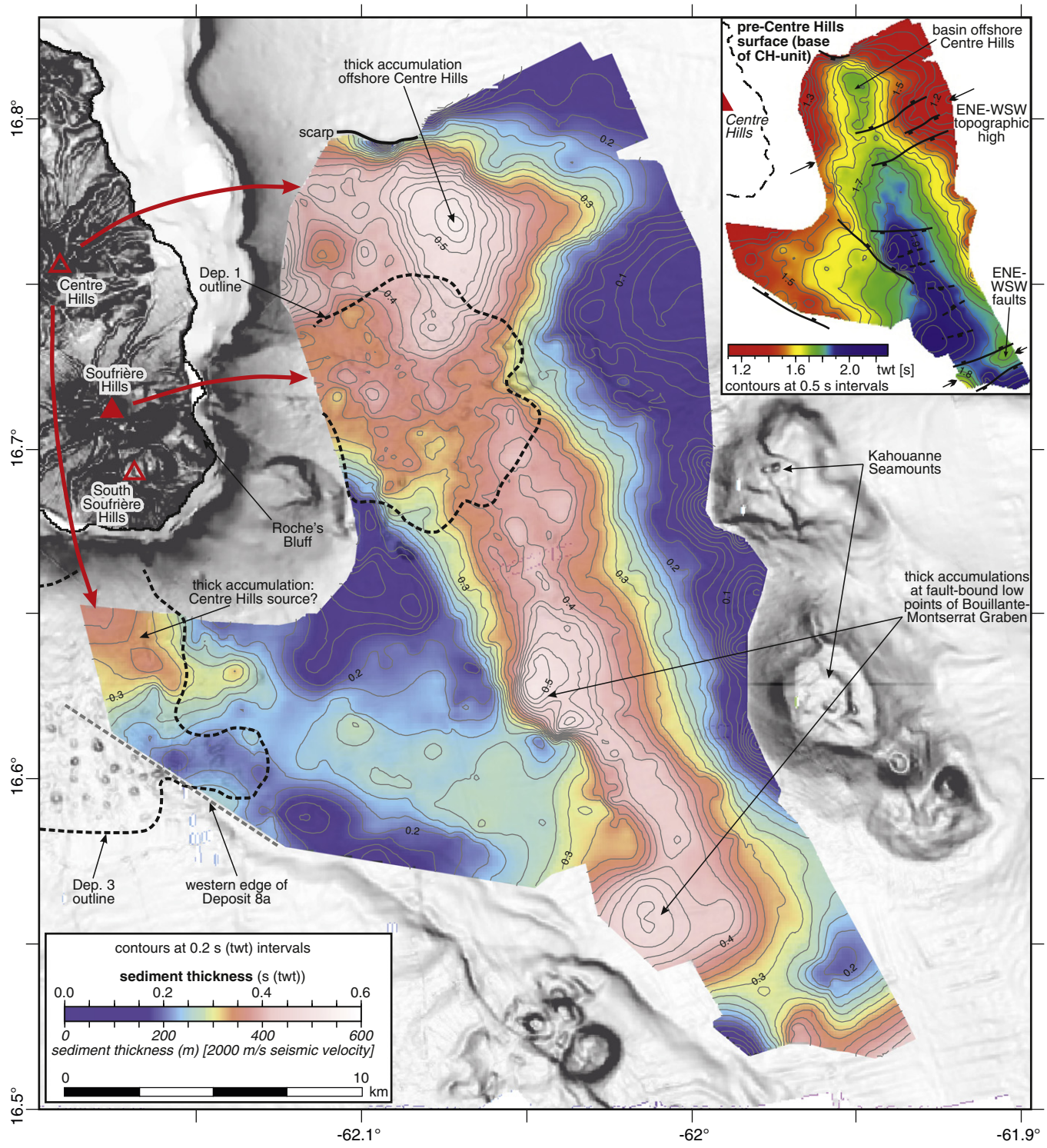

Fig. 18. Isopach map showing sediment thickness above the basal horizon of the CH-unit, mapped across the study area. Interpreted volcanogenic sediment sources are indicated, as are the positions of the surficial Deposits 1 and 3. The inset shows the topography of the basal horizon of the CH-unit, indicating the low points in which sediment accumulation has been most rapid.

from the area (rates of 0.03–0.1 m ka^{-1}) (Reid et al., 1996; Trofimovs et al., 2010), which sample a much shorter time period.

7.3. Landslide timing and island development

Lebas et al. (2011) assumed a sedimentation rate of 0.15 m ka^{-1} within the Bouillante-Montserrat Graben to suggest ages of 233 ka for Deposit 2 and 900 ka for Deposit 8. Our estimates suggest slightly higher long-term sedimentation rates, with the CH-unit surfaces implying that Deposits 2 and 8 have ages of ~140 ka and ~700 ka respectively. We suggest the Lebas et al. (2011) values provide a lower bound on likely deposit ages (Fig. 19). Deposit 4 has a much thinner sedimentary cover than that over Deposit 8 in the main graben, but this is consistent with its position on relatively elevated

Please cite this article as: Watt, S.F.L., et al., Widespread and progressive seafloor-sediment failure following volcanic debris avalanche emplacement: Landslide dynamics and timing offshore Montserrat,..., Marine Geology (2012), http://dx.doi.org/10.1016/j.margeo.2012.08.002

ARTICLE IN PRESS

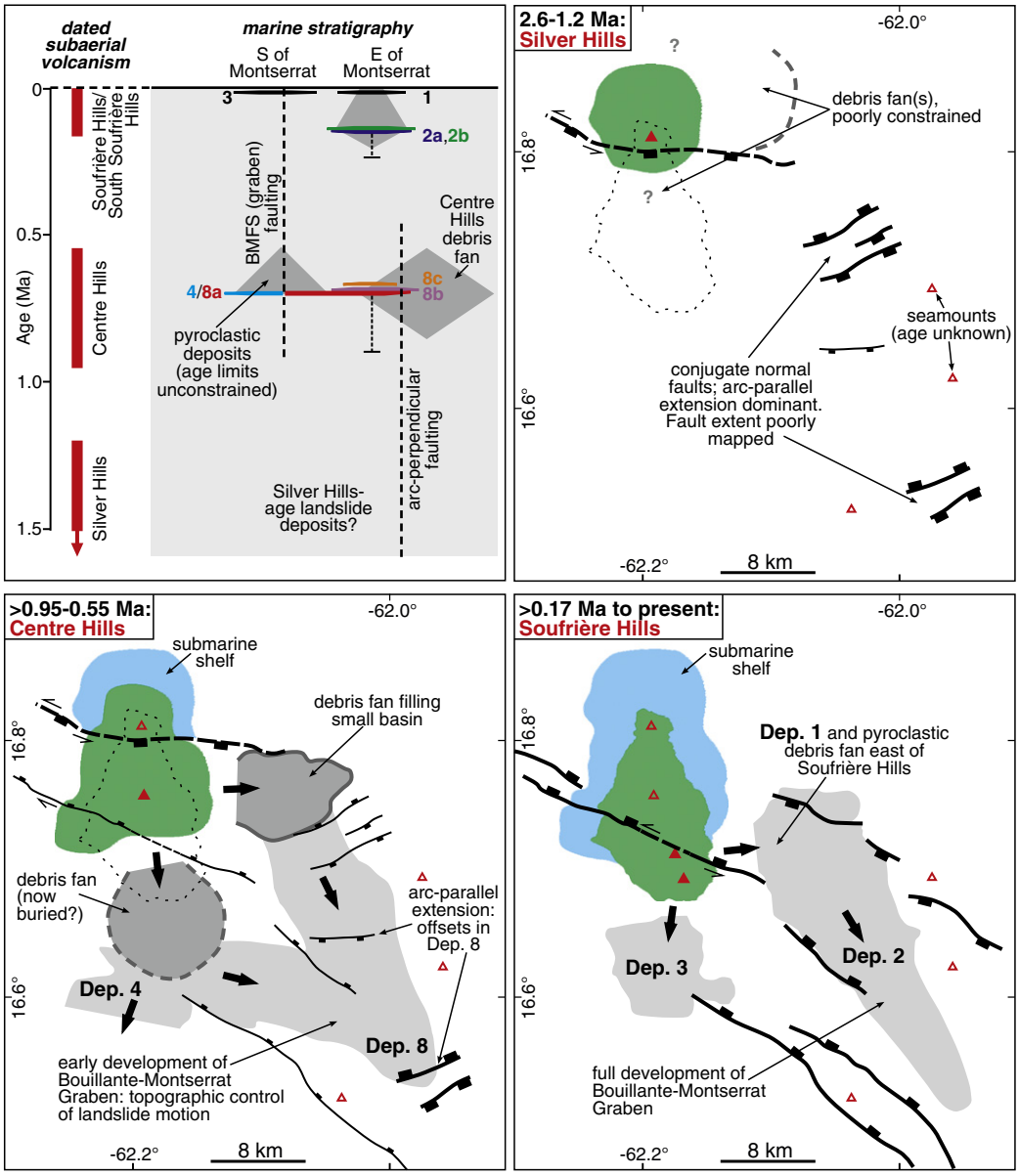

Fig. 19. The proposed development of Montserrat and associated marine landslide deposits. The sketched stratigraphic column shows our estimated deposit ages, with the ages of Lebas et al. (2011) shown as lower bounds for Deposits 2 and 8. In the maps, the subaerial island is marked in green, and the submarine shelf, formed by shoreline erosion (cf. Quartau et al., 2010), in blue. Active faults are taken from Feuillet et al. (2010) and the authors' own interpretation; major faults during any particular time period are highlighted in bold. The dates shown are for subaerial volcanic samples from each of the volcanic centres on Montserrat (Harford et al., 2002). (For interpretation of the references to colour in this figure legend, the reader is referred to the web version of this article.)

seafloor. Using the range of arc-platform sedimentation rates estimated above, the sediment cover (50 m) over the western edge of Deposit 4 suggests its age falls between 1.7 and 0.5 Ma. Although this is an imprecise estimate, it provides additional confirmation that a direct link between Deposits 4 and 8 is plausible.

It is notable that the two largest landslides at Montserrat (Deposits 2 and 8) were derived from different volcanic centres. These largest events occurred relatively early during periods of elevated offshore volcaniclastic sedimentation, being overlain (and to some extent, underlain) by the pyroclastic facies (Fig. 9) and other, smaller flank collapse deposits. However, in the main Bouillante-Montserrat Graben Deposits 2 and 8 are separated by ~200 m of seafloor sediment, corresponding to a gap in offshore volcaniclastic sedimentation. This relationship is consistent with a cyclic timescale of volcanic edifice growth and destruction at Montserrat (Fig. 19). Periods of edifice maturity are marked by large flank collapses in their early stages and deposit large volumes of volcaniclastic sediment offshore. Large, early flank collapses are capable of mobilising even larger volumes of seafloor sediment (if emplaced on such material), whereas later collapses simply add to a growing volcaniclastic apron around the island flanks. In between these periods of edifice maturity, prolonged gaps of reduced volcaniclastic sedimentation correspond to the constructive phase of a new volcanic centre.

Here, we document two periods of edifice maturity: the older period formed deposits east and south of Centre Hills, including Deposits 4/8a and 8c, while the younger period, associated with the South Soufrière Hills–Soufrière Hills complex, is ongoing, and has produced Deposits 1, 2 and 3, as well as their bounding pyroclastic deposits. We suggest that the sharp upper surface of the debris fan east of Centre Hills (Fig. 17) marks the cessation of Centre Hills

Please cite this article as: Watt, S.F.L., et al., Widespread and progressive seafloor-sediment failure following volcanic debris avalanche emplacement: Landslide dynamics and timing offshore Montserrat,..., Marine Geology (2012), http://dx.doi.org/10.1016/j.margeo.2012.08.002

ARTICLE IN PRESS

volcanism, and the switching of volcanic activity to a new site beneath Soufrière Hills. What controlled this change in the locus of volcanism is unclear, but approximately 0.4 Ma elapsed before the new Soufrière Hills edifice reached sufficient dimensions to undergo large-scale collapse, forming Deposit 2.

In summary, marine volcaniclastic sedimentation around Montserrat has been sporadic. Flank collapses may be relatively closely spaced (i.e. repeat intervals on the order of 10^3 to 10^4 years) during periods of edifice maturity, but widely separated (i.e. repeat intervals of 10^5 to 10^6 years) during the growth of new volcanic centres.

8. Conclusions

The largest landslide deposits off Montserrat involved widespread seafloor-sediment failure triggered by volcanic flank collapse. The largest single event, comprising three sub-units (Deposits 4, 8a and 8b), has a volume of >17 km^3. Of this, Deposits 8a and 8b (>14 km^3) are almost entirely composed of disrupted seafloor sediment. Initial volcanic debris avalanche emplacement, at velocities of ~50 m s^{-1}, incised into and incorporated bedded seafloor-sediment intervals that were up to 100 m thick. This loading initiated adjacent sediment failure, which propagated downslope by deforming a consistent package of in-situ stratigraphy (~70 m in thickness for Deposit 8a) for tens of kilometres, on gradients of $<1°$.

We suggest that seafloor-sediment failure in Deposit 8 was generated by motion of an over-running unit (8b) causing undrained loading of the underlying sediment (8a), with the latter deforming progressively (cf. Voight et al., 2011). This process may have operated in conjunction with the downslope propagation of a basal shear rupture. The margin of Deposit 8 is frontally confined and associated with very little topographic accumulation. Internally, it preserves widespread compressional structures. This suggests that the landslide material was not transported a significant distance, but was disrupted approximately in-situ. Landslides with very similar morphologies occur elsewhere in the Lesser Antilles, and may be relatively common around volcanic islands following debris avalanche emplacement. In general, a range of mechanisms may lead to large-scale progressive failure of marine sediment, without involving extensive disaggregation or downslope sediment transport. This class of landslide is perhaps not widely recognised, and warrants further investigation.

The largest landslide deposits around Montserrat occurred relatively early during stages of edifice maturity (~700 ka for Deposit 8, from Centre Hills, and ~140 ka for Deposit 2, from Soufrière Hills). These stages are characterised by elevated marine volcaniclastic input, while periods in between (e.g., the early growth of Soufrière Hills, over ~0.4 Ma) are marked by much-reduced levels of offshore volcaniclastic sedimentation. The largest landslides at Montserrat, following periods of edifice growth, readily incorporated packages of the parallel-bedded seafloor sediment on which they were emplaced, greatly increasing their overall volume and run-out.

Acknowledgements

We thank the captain and crew of the RRS James Cook and the NMFD technicians for their assistance. This work was funded by the Natural Environment Research Council grant NE/F010478/1. We are grateful to Marc De Batist, Claudia Romagnoli and David Piper for reviews and comments that improved the manuscript.

References

Berndt, C., Costa, S., Canals, M., Camerlenghi, A., De Mol, B., Saunders, M.S., 2012. Repeated slope failure linked to fluid migration: the Ana submarine landslide complex, Eivissa Channel, Western Mediterranean Sea. Earth and Planetary Science Letters 319–210, 65–74.

Boudon, G., Le Friant, A., Komorowski, J.-C., Deplus, C., Semet, M.P., 2007. Volcanic flank instability in the Lesser Antilles Arc: diversity of scale, processes, and temporal recurrence. Journal of Geophysical Research 112, B08205.

Bull, S., Cartwright, J., Huuse, M., 2009. A review of kinematic indicators from mass-transport complexes using 3D seismic data. Marine and Petroleum Geology 26, 1132–1151.

Canals, M., Lastras, G., Urgeles, R., Casamor, J.L., Mienert, J., Cattaneo, A., De Batist, M., Haflidason, H., Imbo, Y., Laberg, J.S., 2004. Slope failure dynamics and impacts from seafloor and shallow sub-seafloor geophysical data: case studies from the COSTA project. Marine Geology 213, 9–72.

Carey, S., Sigurdsson, H., 1984. A model of volcanogenic sedimentation in marginal basins. Geological Society, London, Special Publications 16, 37–58.

Clavero, J.E., Sparks, R.S.J., Huppert, H.E., Dade, W.B., 2002. Geological constraints on the emplacement mechanism of the Parinacota debris avalanche, northern Chile. Bulletin of Volcanology 64, 40–54.

Cole, P.D., Calder, E.S., Sparks, R.S.J., Clarke, A.B., Druitt, T.H., Young, S.R., Herd, R.A., Harford, C.L., Norton, G.E., 2002. Deposits from dome-collapse and fountain-collapse pyroclastic flows at Soufrière Hills Volcano, Montserrat. In: Druitt, T.H., Kokelaar, B.P. (Eds.), The eruption of Soufrière Hills volcano, Montserrat, from 1995 to 1999: Geological Society, London, Memoir, 21, pp. 231–262.

Crandell, D.R., 1989. Gigantic debris avalanche of Pleistocene age from ancestral Mount Shasta volcano, California, and debris-avalanche hazard zonation. United States Geological Survey Bulletin 1861 (32 pp.).

Crandell, D.R., Miller, C.D., Glicken, H.X., Christiansen, R.L., Newhall, C.G., 1984. Catastrophic debris avalanche from ancestral Mount Shasta volcano, California. Geology 12, 143–146.

Davies, T.R., McSaveney, M.J., Hodgson, K.A., 1999. A fragmentation-spreading model for long-runout rock avalanches. Canadian Geotechnical Journal 36, 1096–1110.

Deplus, C., Le Friant, A., Boudon, G., Komorowski, J.C., Villemant, B., Harford, C., Ségoufin, J., Cheminée, J.L., 2001. Submarine evidence for large-scale debris avalanches in the Lesser Antilles Arc. Earth and Planetary Science Letters 192, 145–157.

Druitt, T.H., Kokelaar, B.P., 2002. The eruption of Soufrière Hills volcano, Montserrat, from 1995 to 1999. Geological Society, London, Memoir 21 (645 pp.).

Dufresne, A., Davies, T.R., 2009. Longitudinal ridges in mass movement deposits. Geomorphology 105, 171–181.

Feuillet, N., Manighetti, I., Tapponnier, P., Jacques, E., 2002. Arc parallel extension and localization of volcanic complexes in Guadeloupe, Lesser Antilles. Journal of Geophysical Research 107, 2331.

Feuillet, N., Leclerc, F., Tapponnier, P., Beauducel, F., Boudon, G., Le Friant, A., Deplus, C., Lebrun, J.F., Nercessian, A., Saurel, J.M., 2010. Active faulting induced by slip partitioning in Montserrat and link with volcanic activity: new insights from the 2009 GWADASEIS marine cruise data. Geophysical Research Letters 37, L00E15.

Frey-Martínez, J., Cartwright, J., James, D., 2006. Frontally confined versus frontally emergent submarine landslides: a 3D seismic characterisation. Marine and Petroleum Geology 23, 585–604.

Gafeira, J., Long, D., Scrutton, R., Evans, D., 2010. 3D seismic evidence of internal structure within Tampen Slide deposits on the North Sea Fan: are chaotic deposits that chaotic? Journal of the Geological Society 167, 605–616.

Harford, C.L., Pringle, M.S., Sparks, R.S.J., Young, S.R., 2002. The volcanic evolution of Montserrat using 40Ar/39Ar geochronology. In: Druitt, T.H., Kokelaar, B.P. (Eds.), The Eruption of Soufrière Hills Volcano, Montserrat, from 1995 to 1999: Geological Society, London, Memoir, 21, pp. 93–113.

Hühnerbach, V., Masson, D.G., 2004. Landslides in the North Atlantic and its adjacent seas: an analysis of their morphology, setting and behaviour. Marine Geology 213, 343–362.

Hungr, O., Evans, S.G., 2004. Entrainment of debris in rock avalanches: an analysis of a long run-out mechanism. Bulletin of the Geological Society of America 116, 1240–1252.

Huvenne, V.A.I., Croker, P.F., Henriet, J.P., 2002. A refreshing 3D view of an ancient sediment collapse and slope failure. Terra Nova 14, 33–40.

Iverson, R.M., 1997. The physics of debris flows. Reviews of Geophysics 35, 245–296.

Kenedi, C.L., Sparks, R.S.J., Malin, P., Voight, B., Dean, S., Minshull, T., Paulatto, M., Peirce, C., Shalev, E., 2010. Contrasts in morphology and deformation offshore Montserrat: new insights from the SEA-CALIPSO marine cruise data. Geophysical Research Letters 37, L00E25.

Lambe, T.W., Whitman, R.V., 1969. Soil Mechanics. John Wiley, New York. 553 pp.

Lastras, G., Canals, M., Urgeles, R., Hughes-Clarke, J.E., Acosta, J., 2004. Shallow slides and pockmark swarms in the Eivissa Channel, western Mediterranean Sea. Sedimentology 51, 837–850.

Le Friant, A., Boudon, G., Komorowski, J.C., Deplus, C., 2002. L'île de la Dominique, à l'origine des avalanches de débris les plus volumineuses de l'arc des Petites Antilles. Comptes Rendus Geoscience 334, 235–243.

Le Friant, A., Boudon, G., Deplus, C., Villemant, B., 2003. Large-scale flank collapse events during the activity of Montagne Pelée, Martinique, Lesser Antilles. Journal of Geophysical Research 108, 2055.

Le Friant, A., Harford, C.L., Deplus, C., Boudon, G., Sparks, R.S.J., Herd, R.A., Komorowski, J.C., 2004. Geomorphological evolution of Montserrat (West Indies): importance of flank collapse and erosional processes. Journal of the Geological Society 161, 147–160.

Le Friant, A., Lock, E.J., Hart, M.B., Boudon, G., Sparks, R.S.J., Leng, M.J., Smart, C.W., Komorowski, J.C., Deplus, C., Fisher, J.K., 2008. Late Pleistocene tephrochonology of marine sediments adjacent to Montserrat, Lesser Antilles volcanic arc. Journal of the Geological Society 165, 279–289.

Le Friant, A., Deplus, C., Boudon, G., Sparks, R.S.J., Trofimovs, J., Talling, P., 2009. Submarine deposition of volcaniclastic material from the 1995–2005 eruptions of Soufriere Hills volcano, Montserrat. Journal of the Geological Society 166, 171–182.

Please cite this article as: Watt, S.F.L., et al., Widespread and progressive seafloor-sediment failure following volcanic debris avalanche emplacement: Landslide dynamics and timing offshore Montserrat,..., Marine Geology (2012), http://dx.doi.org/10.1016/j.margeo.2012.08.002

ARTICLE IN PRESS

Le Friant, A., Deplus, C., Boudon, G., Feuillet, N., Trofimovs, J., Komorowski, J.C., Sparks, R.S.J., Talling, P., Loughlin, S., Palmer, M., 2010. Eruption of Soufrière Hills (1995–2009) from an offshore perspective: insights from repeated swath bathymetry surveys. Geophysical Research Letters 37, L11307.
Lebas, E., Le Friant, A., Boudon, G., Watt, S.F.L., Talling, P.J., Feuillet, N., Deplus, C., Berndt, C., Vardy, M.E., 2011. Multiple widespread landslides during the long-term evolution of a volcanic island: insights from high-resolution seismic data, Montserrat, Lesser Antilles. Geochemistry, Geophysics, Geosystems 12, Q05006.
Legros, F., 2002. The mobility of long-runout landslides. Engineering Geology 63, 301–331.
Løvholt, F., Pedersen, G., Gisler, G., 2008. Oceanic propagation of a potential tsunami from the La Palma island. Journal of Geophysical Research 113, C09026.
Mangeney, A., Roche, O., Hungr, O., Mangold, N., Faccanoni, G., Lucas, A., 2010. Erosion and mobility in granular collapse over sloping beds. Journal of Geophysical Research 115, F03040.
Manville, V., Németh, K., Kano, K., 2009. Source to sink: a review of three decades of progress in the understanding of volcaniclastic processes, deposits, and hazards. Sedimentary Geology 220, 136–161.
Masson, D.G., Watts, A.B., Gee, M.J.R., Urgeles, R., Mitchell, N.C., Le Bas, T.P., Canals, M., 2002. Slope failures on the flanks of the western Canary Islands. Earth-Science Reviews 57, 1–35.
Masson, D.G., Harbitz, C.B., Wynn, R.B., Pedersen, G., Løvholt, F., 2006. Submarine landslides: processes, triggers and hazard prediction. Philosophical Transactions of the Royal Society A 364, 2009–2039.
Masson, D.G., Wynn, R.B., Talling, P.J., 2010. Large landslides on passive continental margins: processes, hypotheses and outstanding questions. In: Mosher, D.C., et al. (Ed.), Submarine mass movements and their consequences. Advances in Natural and Technological Hazards Research, vol. 28. Springer, pp. 153–165.
Minisini, D., Trincardi, F., Asioli, A., Canu, M., Foglini, F., 2007. Morphologic variability of exposed mass-transport deposits on the eastern slope of Gela Basin (Sicily channel). Basin Research 19, 217–240.
Moernaut, J., De Batist, M., 2011. Frontal emplacement and mobility of sublacustrine landslides: results from morphometric and seismostratigraphic analysis. Marine Geology 285, 29–45.
Moore, J.G., Normark, W.R., Holcomb, R.T., 1994. Giant Hawaiian landslides. Annual Review of Earth and Planetary Sciences 22, 119–144.
Morita, S., Nakajima, T., Hanamura, Y., 2011. Submarine slump sediments and related dewatering structures: observations of 3D seismic data obtained for the continental slope off Shimokita peninsula, NE Japan. Journal of the Geological Society of Japan 117, 95–98.
Mulder, T., Cochonat, P., 1996. Classification of offshore mass movements. Journal of Sedimentary Research 66, 43–57.
Naranjo, J.A., Francis, P., 1987. High velocity debris avalanche at Lastarria volcano in the north Chilean Andes. Bulletin of Volcanology 49, 509–514.
Paulatto, M., Minshull, T.A., Baptie, B., Dean, S., Hammond, J.O.S., Henstock, T., Kenedi, C.L., Kiddle, E.J., Malin, P., Peirce, C., 2010. Upper crustal structure of an active volcano from refraction/reflection tomography, Montserrat, Lesser Antilles. Geophysical Journal International 180, 685–696.
Petley, D.N., Higuchi, T., Petley, D.J., Bulmer, M.H., Carey, J., 2005. Development of progressive landslide failure in cohesive materials. Geology 33, 201–204.
Pierson, T.C., 1985. Initiation and flow behavior of the 1980 Pine Creek and Muddy river lahars, Mount St. Helens, Washington. Bulletin of the Geological Society of America 96, 1056–1069.
Prior, D.B., Bornhold, B.D., Johns, M.W., 1984. Depositional characteristics of a submarine debris flow. Journal of Geology 92, 707–727.
Puzrin, A.M., Germanovich, L.N., Kim, S., 2004. Catastrophic failure of submerged slopes in normally consolidated sediments. Geotechnique 54, 631–643.
Quartau, R., Trenhaile, A.S., Mitchell, N.C., Tempera, F., 2010. Development of volcanic insular shelves: insights from observations and modelling of Faial Island in the Azores Archipelago. Marine Geology 275, 66–83.
Reid, R.P., Carey, S.N., Ross, D.R., 1996. Late Quaternary sedimentation in the Lesser Antilles island arc. Bulletin of the Geological Society of America 108, 78–100.
Richards, J.P., Villeneuve, M., 2001. The Llullaillaco volcano, northwest Argentina: construction by Pleistocene volcanism and destruction by sector collapse. Journal of Volcanology and Geothermal Research 105, 77–105.
Satake, K., Kato, Y., 2001. The 1741 Oshima Oshima Eruption: extent and volume of submarine debris avalanche. Geophysical Research Letters 28, 427–430.
Schnellman, M., Anselmetti, F.S., Giardini, D., McKenzie, J.A., 2005. Mass movement-induced fold-and-thrust belt structures in unconsolidated sediments in Lake Lucerne (Switzerland). Sedimentology 52, 271–289.
Shea, T., van Wyk de Vries, B., Pilato, M., 2008. Emplacement mechanisms of contrasting debris avalanches at Volcán Mombacho (Nicaragua), provided by structural and facies analysis. Bulletin of Volcanology 70, 899–921.
Siebert, L., 1984. Large volcanic debris avalanches: characteristics of source areas, deposits, and associated eruptions. Journal of Volcanology and Geothermal Research 22, 163–197.
Siebert, L., Glicken, H., Ui, T., 1987. Volcanic hazards from Bezymianny- and Bandai-type eruptions. Bulletin of Volcanology 49, 435–459.
Sigurdsson, H., Sparks, R.S.J., Carey, S.N., Huang, T.C., 1980. Volcanogenic sedimentation in the Lesser Antilles arc. Journal of Geology 88, 523–540.
Stoopes, G.R., Sheridan, M.F., 1992. Giant debris avalanches from the Colima Volcanic Complex, Mexico: implications for long-runout landslides (>100 km) and hazard assessment. Geology 20, 299–302.
Trincardi, F., Argnani, A., 1990. Gela submarine slide: a major basin-wide event in the Plio-Quaternary foredeep of Sicily. Geo-Marine Letters 10, 13–21.
Tripsanas, E.K., Piper, D.J.W., Jenner, K.A., Bryant, W.R., 2008. Submarine mass-transport facies: new perspectives on flow processes from cores on the eastern North American margin. Sedimentology 55, 97–136.
Trofimovs, J., Amy, L., Boudon, G., Deplus, C., Doyle, E., Fournier, N., Hart, M.B., Komorowski, J.C., Le Friant, A., Lock, E.J., Pudsey, C., Ryan, G., Sparks, R.S.J., Talling, P.J., 2006. Submarine pyroclastic deposits formed at the Soufrière Hills volcano, Montserrat (1995–2003): what happens when pyroclastic flows enter the ocean? Geology 34, 549–552.
Trofimovs, J., Sparks, R.S.J., Talling, P.J., 2008. Anatomy of a submarine pyroclastic flow and associated turbidity current: July 2003 dome collapse, Soufriere Hills volcano, Montserrat, West Indies. Sedimentology 55, 617–634.
Trofimovs, J., Fisher, J.K., Macdonald, H.A., Talling, P.J., Sparks, R.S.J., Hart, M.B., Smart, C.W., Boudon, G., Deplus, C., Komorowski, J.C., Le Friant, A., Moreton, S.G., Leng, M.J., 2010. Evidence for carbonate platform failure during rapid sea level rise; ca 14 000 year old bioclastic flow deposits in the Lesser Antilles. Sedimentology 57, 735–759.
Trofimovs, J., Foster, C., Sparks, R.S.J., Loughlin, S., Le Friant, A., Deplus, C., Porritt, L., Christopher, T., Luckett, R., Talling, P.J., Palmer, M.R., Le Bas, T., 2011. Submarine pyroclastic deposits formed during the 20th May 2006 dome collapse of the Soufrière Hills Volcano, Montserrat. Bulletin of Volcanology. http://dx.doi.org/10.1007/s00445-011-0533-5.
Vallance, J.W., Scott, K.M., 1997. The Osceola Mudflow from Mount Rainier: sedimentology and hazard implications of a huge clay-rich debris flow. Geological Society of America Bulletin 109, 143–163.
Van Der Merwe, W.C., Hodgson, D.M., Flint, S.S., 2011. Origin and terminal architecture of a submarine slide: a case study from the Permian Vischkuil formation, Karoo basin, South Africa. Sedimentology. http://dx.doi.org/10.1111/j.1365-3091.2011.01249.x.
Viesca, R.C., Rice, J.R., 2010. Modeling slope instability as shear rupture propagation in a saturated porous medium. In: Mosher, D.C., et al. (Ed.), Submarine mass movements and their consequences. Advances in Natural and Technological Hazards Research, vol. 28. Springer, pp. 215–225.
Voight, B., Elsworth, D., 1997. Failure of volcano slopes. Geotechnique 47, 1–31.
Voight, B., Janda, R.J., Glicken, H., Douglass, P.M., 1983. Nature and mechanics of the Mount St Helens rockslide-avalanche of 18 May 1980. Geotechnique 33, 243–273.
Voight, B., Le Friant, A., Boudon, G., Deplus, C., Komorowski, J.C., Lebas, E., Sparks, R.S.J., Talling, P., Trofimovs, J., 2011. Undrained sediment loading key to long-runout submarine mass movements: evidence from the Caribbean volcanic arc. In: Yamada, Y., et al. (Ed.), Submarine mass movements and their consequences. Advances in Natural and Technological Hazards Research, vol. 31. Springer, pp. 417–428.
Wadge, G., Herd, R., Ryan, G., Calder, E.S., Komorowski, J.C., 2010. Lava production at Soufrière Hills Volcano, Montserrat: 1995–2009. Geophysical Research Letters 37, L00E03.
Ward, S.N., Day, S., 2001. Cumbre Vieja Volcano — potential collapse and tsunami at La Palma, Canary Islands. Geophysical Research Letters 28, 3397–3400.
Ward, S.N., Day, S., 2003. Ritter Island Volcano — lateral collapse and the tsunami of 1888. Geophysical Journal International 154, 891–902.
Watt, S.F.L., Talling, P.J., Vardy, M.E., Heller, V., Hühnerbach, V., Urlaub, M., Sarkar, S., Masson, D.G., Henstock, T.J., Minshull, T.A., Paulatto, M., Le Friant, A., Lebas, E., Berndt, C., Crutchley, G.J., Karstens, J., Stinton, A.J., Maeno, F., 2012. Combinations of volcanic-flank and seafloor-sediment failure offshore Montserrat, and their implications for tsunami generation. Earth and Planetary Science Letters 319–320, 228–240.
Watts, A.B., Masson, D.G., 2001. New sonar evidence for recent catastrophic collapses of the north flank of Tenerife, Canary Islands. Bulletin of Volcanology 63, 8–19.
Waythomas, C.F., Watts, P., Shi, F., Kirby, J.T., 2009. Pacific Basin tsunami hazards associated with mass flows in the Aleutian arc of Alaska. Quaternary Science Reviews 28, 1006–1019.

Please cite this article as: Watt, S.F.L., et al., Widespread and progressive seafloor-sediment failure following volcanic debris avalanche emplacement: Landslide dynamics and timing offshore Montserrat,..., Marine Geology (2012), http://dx.doi.org/10.1016/j.margeo.2012.08.002